Journal Name

RSCPublishing

COMMUNICATION

Electronic Supporting Information for:

Fused Bis-Azacalixphyrins that Reaches NIR-II Absorptions

Lucien Lavaud,[a] Cloé Azarias,[b,c] Gabriel Canard,*[a] Simon Pascal,[a] Joachim Galiana,[a] Michel Giorgi,[d] Zhongrui Chen,[a] Denis Jacquemin*[b] and Olivier Siri*[a]

[a] *Aix Marseille Univ, CNRS, CINaM, UMR 7325, 13288, Marseille, France. Fax: (+33) 491 41 8916; E-mails: gabriel.canard@univ-amu.fr and olivier.siri@ univ-amu.fr.*

[b] *Laboratoire CEISAM, UMR CNRS 6230, Université de Nantes, 2, rue de la Houssinière, 44322 Nantes, France. Email: Denis.Jacquemin@univ-nantes.fr.*

[c] *Present address : LaboLife France, 1, rue François Bruneau, 44000 Nantes, France.*

[d] *Aix Marseille Univ, CNRS, Centrale Marseille, FSCM, Spectropole, Marseille, France.*

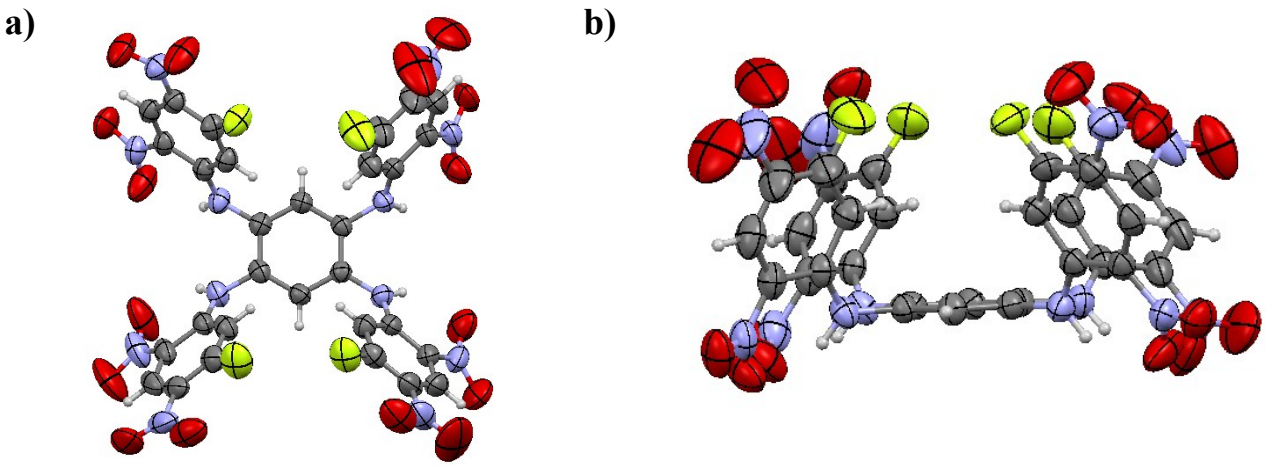

Fig S1. ORTEP views of the [1+4] adduct **9** (Solvent molecules are omitted for clarity).

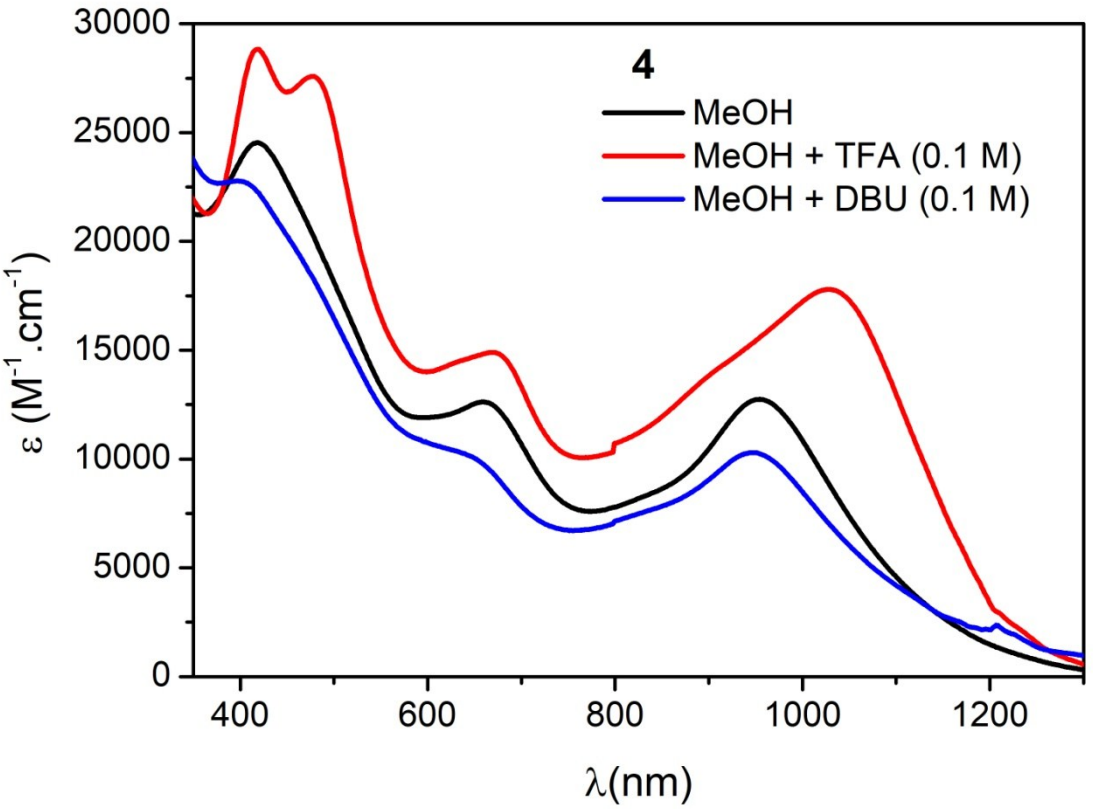

Fig S2. UV-Vis-NIR electronic absorption spectra of the bis-ACP **4** in neutral, acidic and basic MeOH.

Synthetic protocols

Reagents. All reagents were purchased from Alfa-Aesar and used as received. Column chromatography was performed using Silica 60M (0.04-0.063 mm) purchased from Macherey-Nagel. Optical properties were recorded in spectrophotochemical grade solvents.

Analytical methods and apparatus. NMR spectra were recorded on a JEOL ECS400 NMR spectrometer at room temperature. NMR chemical shifts are given in ppm (δ) relative to Me_4Si with solvent resonances used as internal standards (CD_2Cl_2: 5.32 ppm for ^1H and 53.84 for ^{13}C; DMSO-d_6: 2.50 ppm for ^1H and 39.52 for ^{13}C). UV-Vis-NIR absorption spectra were recorded on a VARIAN CARY 50 SCAN and VARIAN CARY 5000 SCAN spectrophotometers at room temperature. HRMS (ESI) and MS (ESI) analyses were performed on a QStar Elite (Applied Biosystems SCIEX) spectrometer or on a SYNAPT G2 HDMS (Waters) spectrometer by the "*Spectropole*" of Aix Marseille University. These two instruments are equipped with an ESI or MALDI source. Infrared spectra were recorded on a Agilent Cary 630 FTIR equipped with an attenuated total reflectance (ATR) sampling.

Single Crystal X-ray Diffraction. Suitable crystals for compounds **9** were obtained by slow diffusion of Diethyl Ether in a concentrated DMSO solution of **9**. The intensity data for **9** were collected on a Bruker–Nonius KappaCCD diffractometer using MoKα radiation (λ=0.71073 Å). Data collection was performed with COLLECT[3], cell refinement and data reduction with DENZO/SCALEPACK[4]. The structure was solved with SIR92[5] and SHELXL[6] was used for full matrix least squares refinement. The hydrogen atoms were all introduced at geometrical positions except the H-atoms for the N(H) that were found experimentally and their Uiso parameters were fixed to 1.2Ueq(parent atom) for the C(H) and N(H) and to 1.5Ueq(parent atom) for the CH_3. Compound **9** co-crystallized with 5 disordered molecules of DMSO. Suitable crystals for compounds **10** were obtained by slow evaporation of a DCM-Acetone solution of **10**. The single crystal of **10** was mounted on a Rigaku Oxford Diffraction SuperNova diffractometer and measured at 293K at the Cu radiation (λ=1.54184 Å). Data collection, reduction and multiscan ABSPACK correction were performed with CrysAlisPro (Rigaku Oxford Diffraction). Using Olex2[7] the structures were solved by direct methods with SHELXT[8] and SHELXL[6] was used for full matrix refinements. All H-atoms were found experimentally and their coordinates and Uiso parameters were constrained to 1.5Ueq(parent atom) for the methyls and to 1.2Ueq(parent atom) for the other carbons and amines. CCDC 1905517 (**9**) and CCDC 1905518 (**10**) contain the supplementary crystallographic data for this paper and are provided free of charge by The Cambridge Crystallographic Data Centre.

Dioctyl TAB 5a

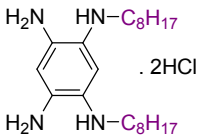

In a glass tube, compound 1,3-dinitro-4,6-dioctylaminobenzene[1] (2 g, 4.73 mmol, 1 equiv.) and iron powder (1.32 g, 23.67 mmol, 5 equiv.) were dissolved in 20 mL of a DCM and 20 mL of HCl 12 N. The tube was sealed and the mixture was stirred vigorously for 64 hours, then the precipitate was filtered and rinsed with concentrated HCl and DCM. The solid was sonicated in concentrated HCl for 30 min, filtered again on a sintered glass. The filtrate was removed from the Buchner, and the solid was dissolved in a MeOH/HCl mixture (7:3) through the sintered glass filter. The filtrate was concentrated under reduce pressure, then the residue was filtered again, rinsed with HCl (12 M), DCM and Et_2O. The solid was finally dried under vacuum to afford the product **5a** as a white solid (1.46 g, 3.35 mmol, 71%). The compound was stored at -20 °C. Spectral and physicochemical properties concur with published data.[2]

^{1}H NMR (400 MHz, DMSO-d$_6$): δ = 6.92 (br s, 1H), 6.66 (br s, 1H), 3.07 (t, ^3J (H,H)= 7.5 Hz, 4H, NCH_2), 1.63 (quint, ^3J (H,H)= 7.5 Hz, 4H, CH_2), 1.35-1.24 (m, 20H, CH_2), 0.84 (t, ^3J (H,H)= 7.2 Hz, 6H, CH_3). No ^{13}C NMR spectrum of **5a** could be recorded owing to its poor stability in solution.

N^1,N^2,N^4,N^5-tetrakis(5-fluoro-2,4-dinitrophenyl)benzene-1,2,4,5-tetraamine 9

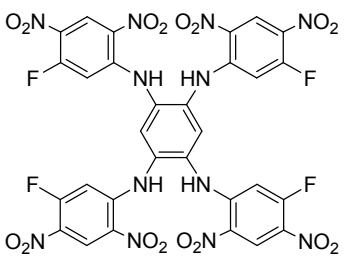

To a solution of 1,5-difluoro-2,4-dinitrobenzene **6** (2.0 g, 9.6 mmol, 5.3 equiv.) in degassed THF (200 mL), was added 1,2,4,5-tetraaminobenzene tetra-hydrochloride **5b** (0.5 g, 1.8 mmol, 1.0 equiv.) under an argon atmosphere. Then degassed DIPEA (2.5 mL, 25 mmol, 14 equiv.) was added dropwise at 0 °C. The solution was stirred at 0 °C for 1 hour, at room temperature during 1 h, and finally heated to reflux

overnight (16 h). THF was evaporated and the crude product was filtered, washed successively with EtOH and three times with 20 mL of acetone to afford **9** as an orange powder (0.543 g, 0.6 mmol, 33%).

^{1}H NMR (400 MHz, DMSO-d$_6$): δ = 10.23 (br s, 4H), 8.88 (d, ^4J (H,F) = 7.8 Hz, 4H), 7.87 (s, 2H), 7.43 (d, ^3J (H,F)= 13.8 Hz, 4H). No ^{13}C NMR spectrum of **9** could be recorded owing to its poor solubility. **HRMS (ESI-TOF):** calcd. for $C_{30}H_{13}N_{12}O_{16}F_4^-$ ([M-H]$^-$) 873.0514, found 873.0510. **IR (neat, cm^{-1}):** 3305, 3278, 3084, 1621, 1546, 1581, 1504, 1426, 1363, 1324, 1301, 1270, 1220, 1180, 1126, 1054, 936, 880, 854, 832, 741, 708.

Fused azacalixarene 10

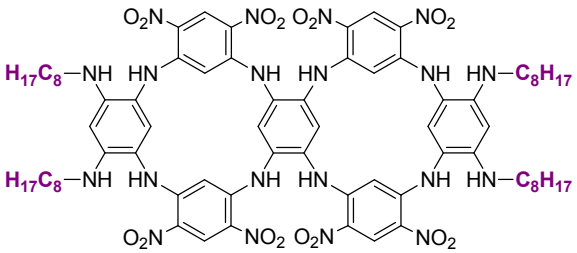

To a solution of **9** (200 mg, 0.228 mmol, 1 equiv.) in degassed MeCN (25 mL), was added 1,2-dioctylamino-4,5-diaminobenzene di-hydrochloride **5a** (209 mg, 0.480 mmol, 2.1 equiv.) under an argon atmosphere. Then degassed DIPEA (320 µL, 1.824 mmol, 8 equiv.) was added dropwise at 0 °C. The solution was stirred 1 hour at room temperature and finally heated to reflux overnight. After evaporation of the solvent, the resulting solid was washed successively by ethanol and dichloromethane. The dichloromethane filtrate was evaporated and the resulting residue was purified on column chromatography (SiO_2, DCM/Et_2O 9:1 to 10:0) to afford the product **10** as dark solid (134 mg, 88.2 µmol, 38%).

Rf= 0.14 (DCM/Et_2O 9:1). **^{1}H NMR (400 MHz, CD$_2$Cl$_2$)**: 9.33 (s, 4H, NH), 9.25 (s, 4H, ArH), 9.10 (s, 4H, NH), 7.36 (s, 2H, ArH), 6.72 (s, 2H, ArH), 5.86 (s, 2H, Ar), 5.72 (s, 4H, ArH), 4.08 (br s, 4H, NH), 3.01 (m, 8H, CH_2), 1.48-1.52 (m, 8H, CH_2), 1.25-1.29 (m, 40H, CH_2), 0.86 (t, ^3J (H,H)= 7.1 Hz, 12H, CH_3). **^{13}C NMR (100 MHz, CD$_2$Cl$_2$):** δ = 150.82 (C^{IV}), 147.01 (C^{IV}), 146.56 (C^{IV}), 134.51 (C^{IV}), 129.67 (CH), 129.19 (CH), 128.06 (CH), 126.31 (C^{IV}), 125.51 (C^{IV}), 110.01 (C^{IV}), 94.98 (CH), 93.10 (CH), 43.90 (CH_2), 32.21 (CH_2), 29.77 (CH_2), 29.65 (CH_2), 29.55 (CH_2), 27.52 (CH_2), 23.04 (CH_2), 14.24 (CH_3). **HRMS (ESI-TOF):** calcd. for $C_{74}H_{93}N_{20}O_{16}^-$ ([M-H]$^-$) 1517.7084, found 1517.7075. **IR (neat, cm^{-1}):** 3409, 3336, 3094, 2920, 2846, 1611, 1567, 1518, 1466, 1406, 1341, 1321, 1284, 1240, 1196, 1067, 924, 888, 831, 744, 688.

Fused azacalixphyrin 4

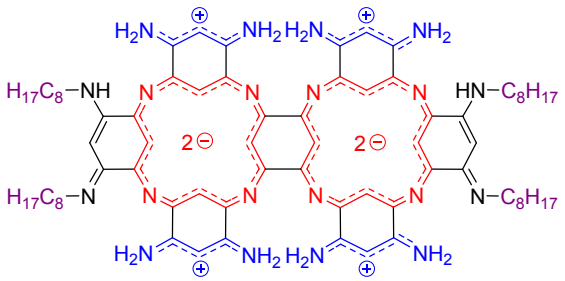

Compound **10** (40 mg, 26 µmol, 1 equiv.), Pd on carbon (10 %, 10 mg, 9.43 µmol, 0.36 equiv.) and THF (15 mL) were introduced into a pressure bomb. Then hydrazine monohydrate (159.8 µL, 3.3 mmol, 127 equiv.) was added to the mixture before closing the bomb by a Teflon seal. The mixture was stirred at 150 °C for 24 hours. The mixture was diluted by MeOH (50 mL) before air was bubbled in the mixture for 22 hours. After evaporation of the solvents, the residue was purified using an alumina pad (alumina 90 neutral, Merck© grade I, DCM/MeOH 9:1). After evaporation of the solvents and precipitation from a MeOH/diethyl ether mixture, the solid was washed successively by petroleum ether and dichloromethane to yield **4** as a dark solid (10 mg, 7.88 µmol, 30 %).

HRMS (MALDI-TOF): calcd. for $C_{74}H_{101}N_{20}^{+}$ ($[M+H]^{+}$) 1269.8513, found 1269.8496. **IR (neat, cm^{-1}):** 3138, 2919, 2847, 1617, 1507, 1457, 1358, 1277, 1195, 1061, 832, 718. **^{13}C solid NMR (100 MHz):** δ (ppm) = 14.5, 23.3, 29.9, 44.4, 94.4, 101.0, 109.5, 130.0, 141.2, 155.7. **UV-vis-NIR (MeOH + 0.1 M TFA, 25 °C):** λ /nm (ε / M^{-1}cm^{-1}) = 1029 (17800), 668 (14900), 478 (27600), 418 (28800), 309 (25300).

^{1}H and ^{13}C NMR spectra

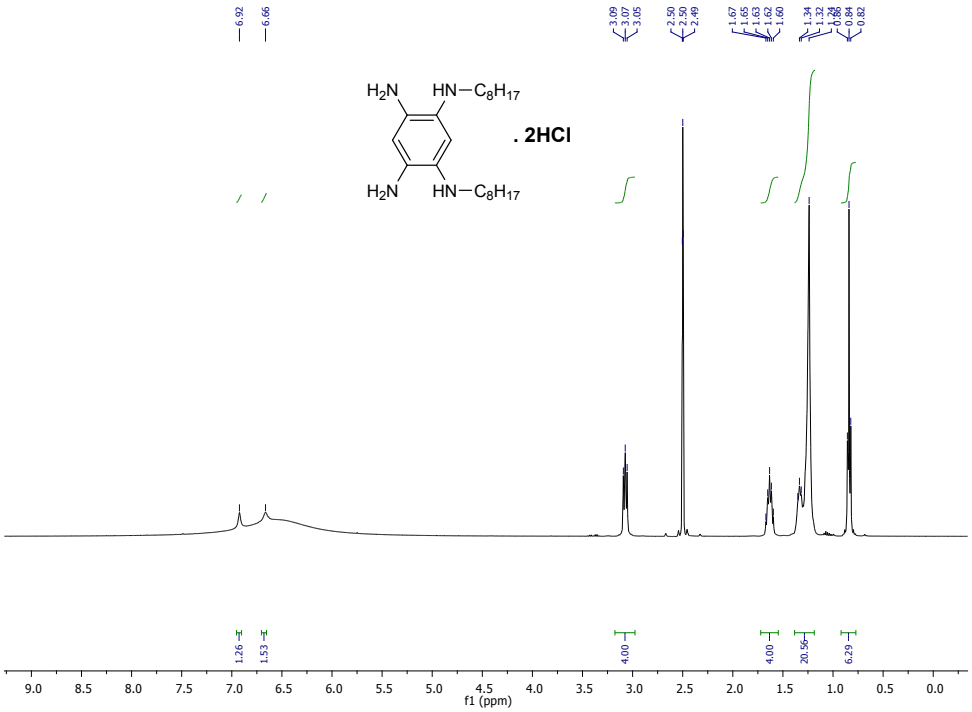

Fig. S3: ^{1}H NMR spectrum of **5a** in DMSO-d_6 (400 MHz)

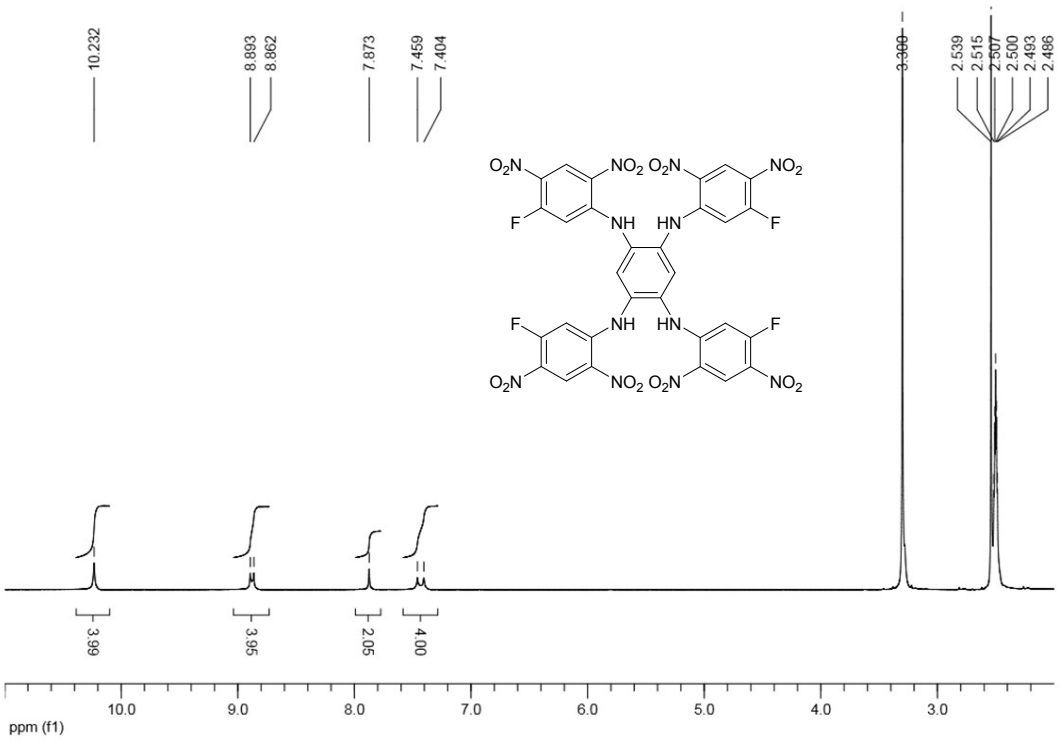

Fig. S4: ^{1}H NMR spectrum of **9** in DMSO-d_6 (400 MHz)

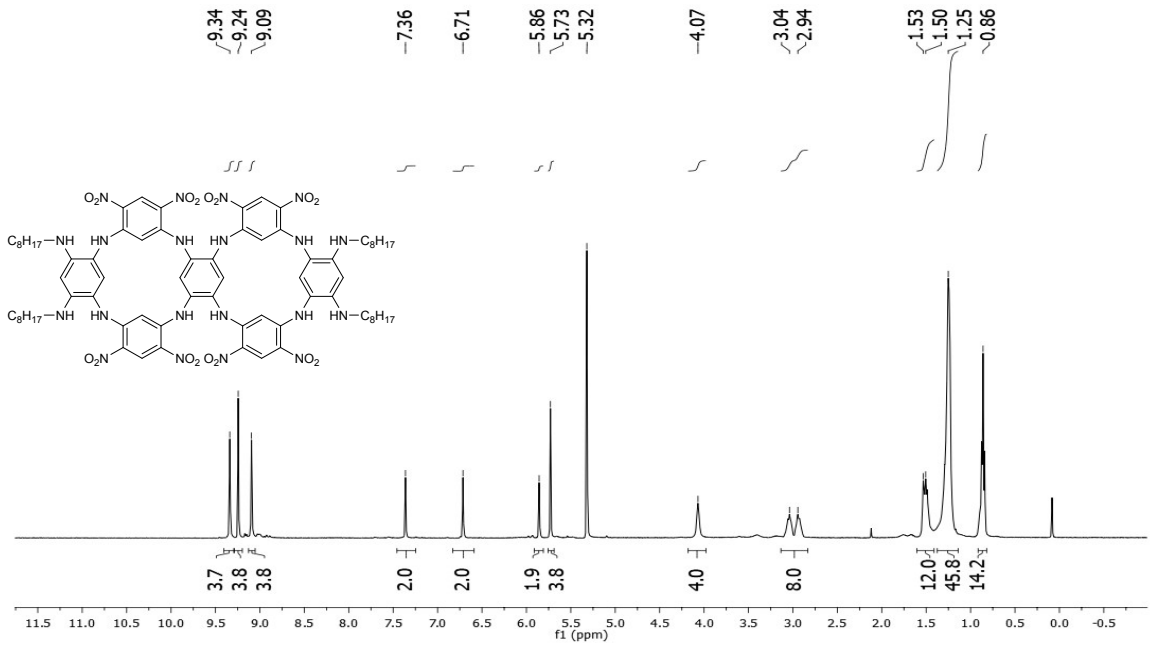

Fig. S5: ^{1}H NMR spectrum of **10** in CD_2Cl_2 (400 MHz)

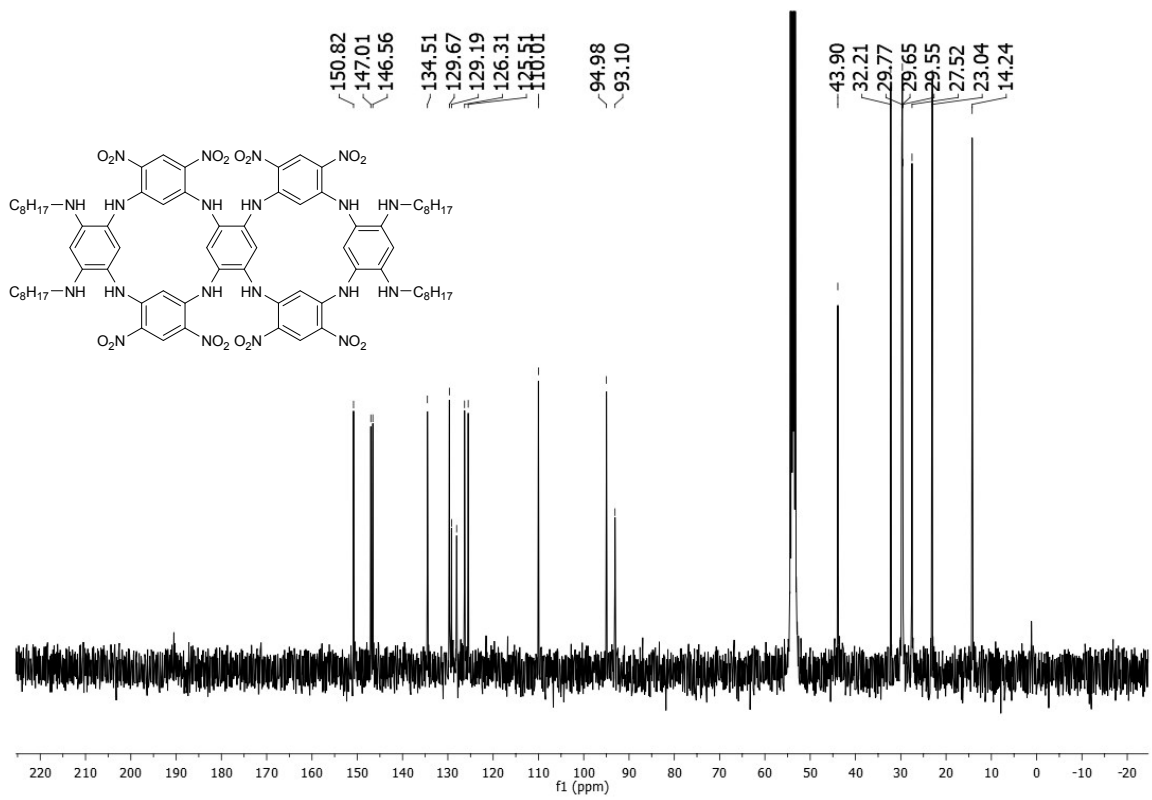

Fig. S6: ^{13}C NMR spectrum of **10** in CD_2Cl_2 (100 MHz)

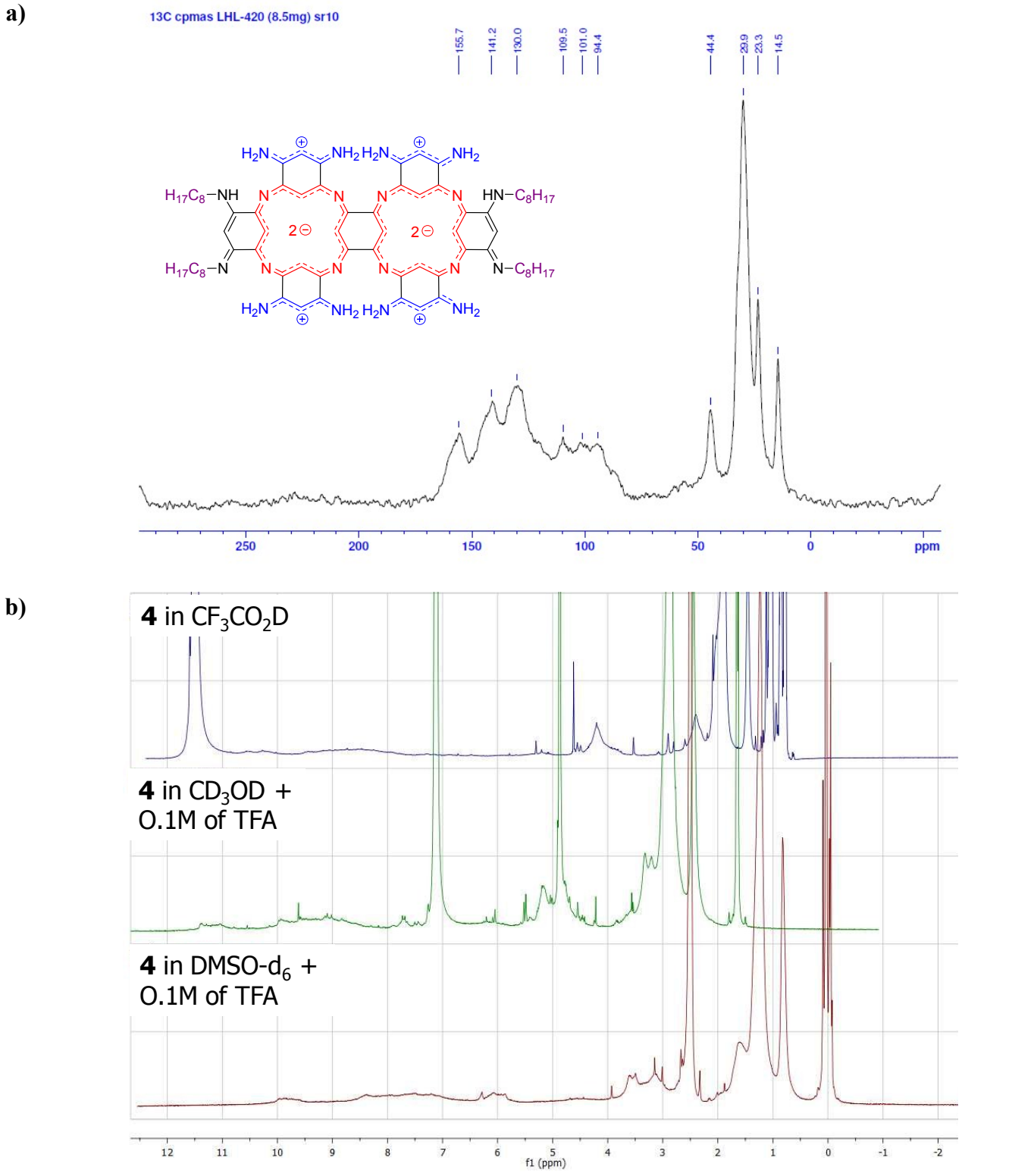

Fig. S7: a) ^{13}C solid state NMR spectrum of **4** (100 MHz) and b) ^{1}H NMR spectra of **4** (400 MHz) in deuterated TFA, in MeOD containing 0.1M of TFA and in d_6-DMSO containing 0.1M of TFA.

Mass spectra

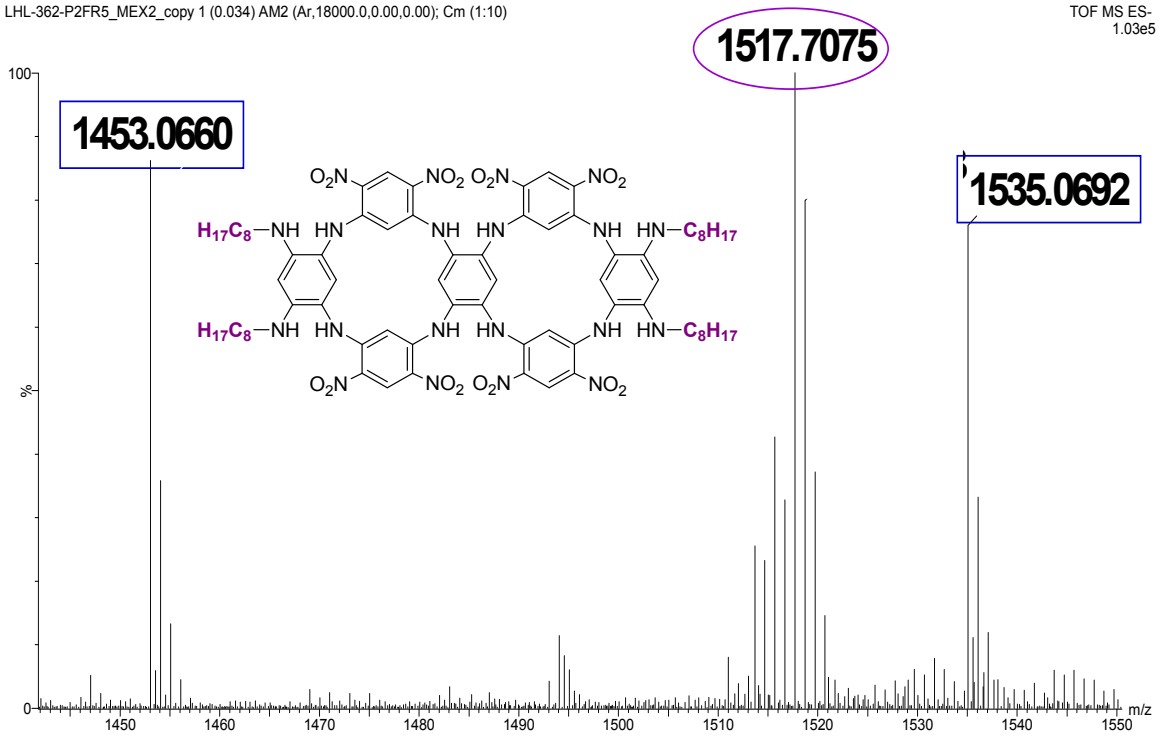

Fig. S8: HRMS (ESI) mass spectrum of **10**

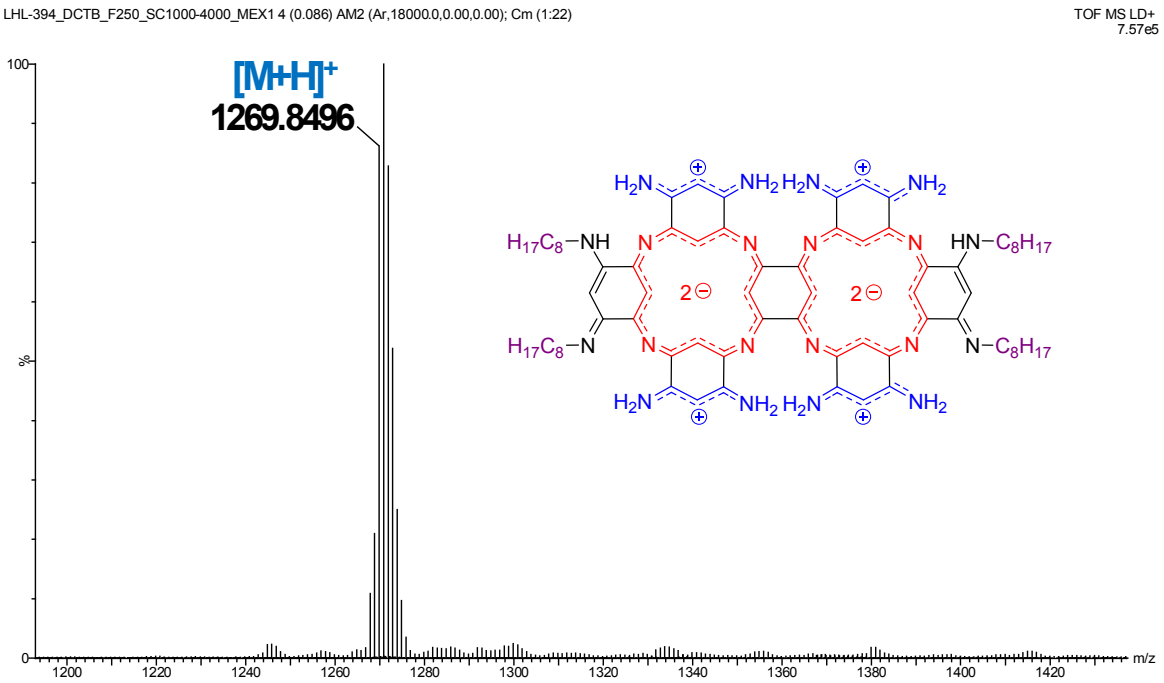

Fig. S9: HRMS (MALDI-TOF) mass spectrum of **4**

Infrared spectra

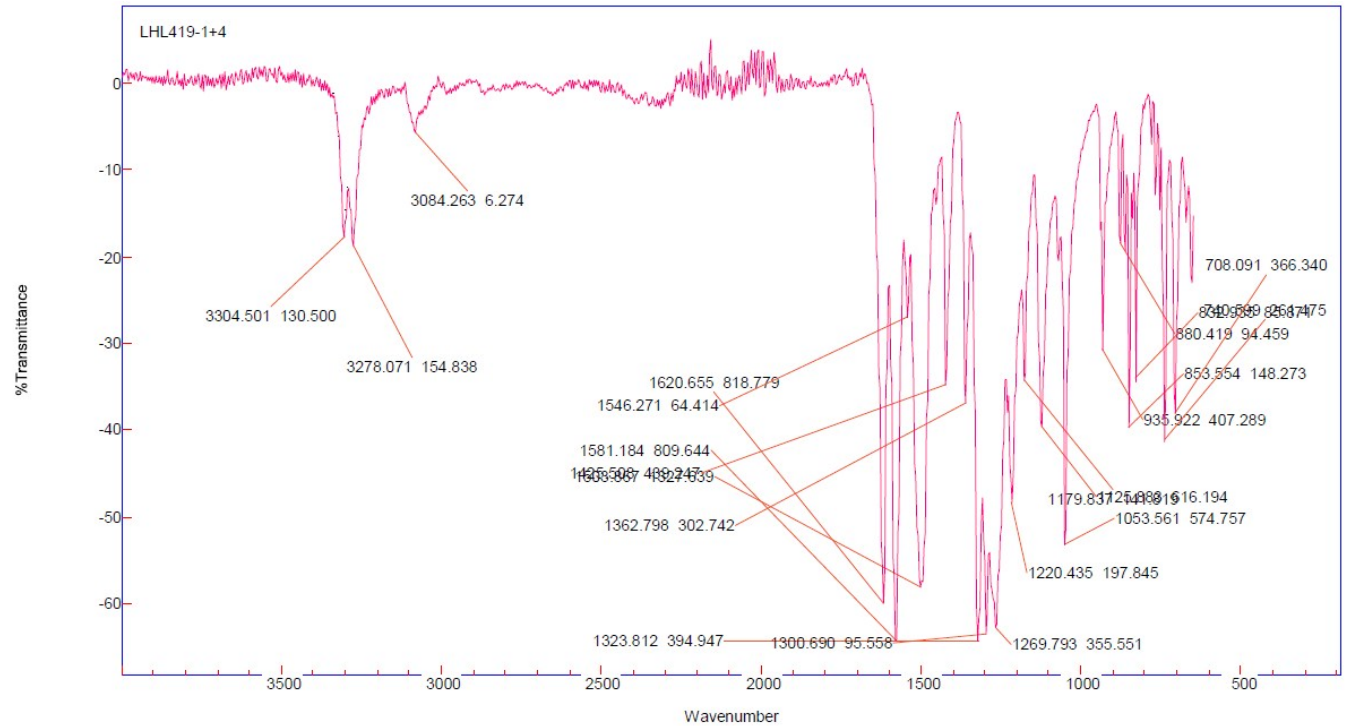

Fig. S10: Infrared spectrum of compound **9**

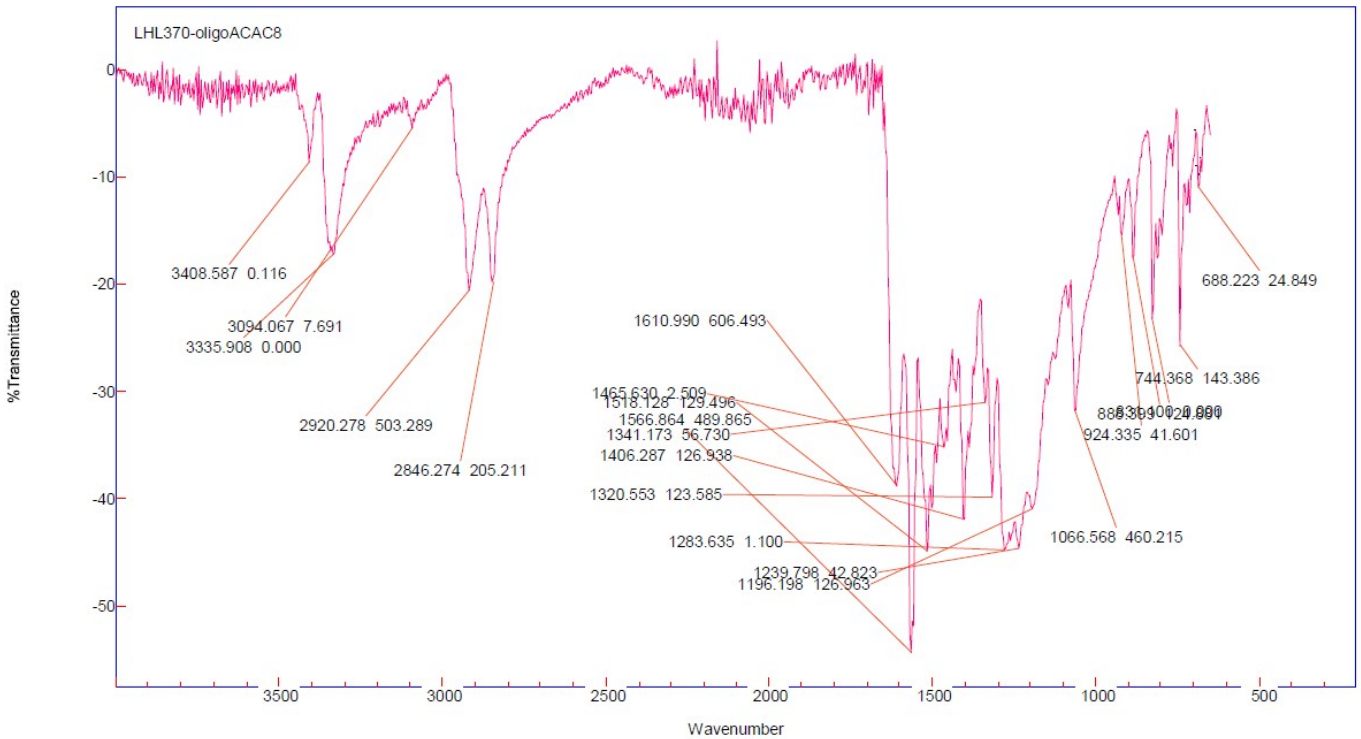

Fig. S11: Infrared spectrum of compound **10**

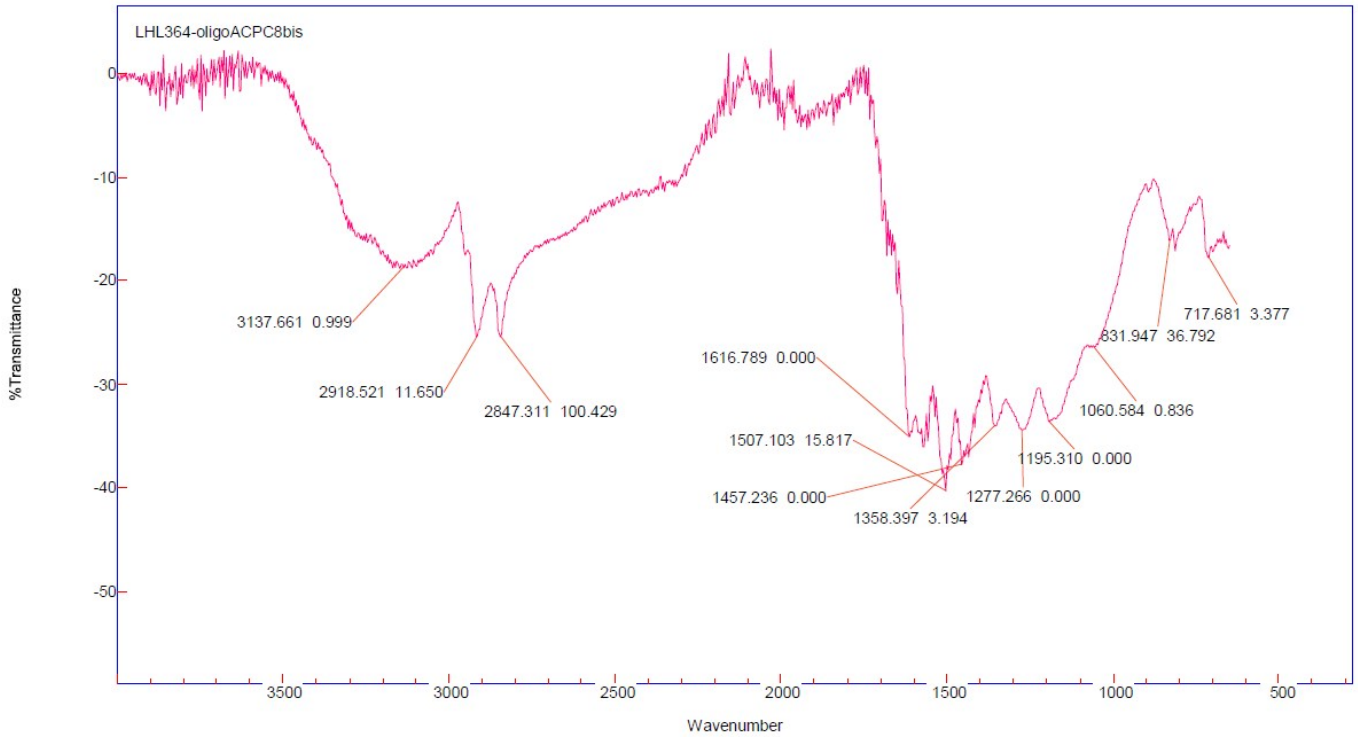

Fig. S12: Infrared spectrum of compound **4**

Theoretical Section: from **5a** to **10**

Methods. All DFT calculations have been performed using Gaussian09/16 programs.[9] The self-consistent field (10^{-10} a.u.) and geometry optimization (10^{-10} a.u.) convergence thresholds have been tightened and an accurate (*99,590*) pruned DFT integration grid has been used. All the DFT calculations relied on the PBE0[10] hybrid functional and have been performed in gas phase. Except when explicitly noted, dispersion corrections as given by the so-called $D3^{BJ}$ model[11] have been included. The optimization and frequency calculations have been determined with a small basis set (SBS), 6-31G(d). The same approach was selected to confirm the nature of all ground states (transition states) that returned 0 (1) imaginary vibrational modes, and to access the free energies *G*. On the basis of these optimized geometries, a larger basis set (LBS), that is, 6-311+G(2d,p) was used to compute: (i) the total electronic energy (*E*) in order to correct the free energies G^{SBS} obtained from the frequency calculations for the basis set effect, using: $G^{LBS} = G^{SBS} + E^{LBS} - E^{SBS}$; (ii) the atomic charges using the Merz-Kollman (MK)[12] and the CHelpG[13] schemes, for both the neutral and cationic forms. The NMR spectra of the most stable conformers of the fused-azacalix[4]arene have also been computed. For these calculations, all structures have been re-optimized in dichloromethane (DCM) using the PCM-PBE0- $D3^{BJ}$/6-31G(d) level of theory and the NMR shieldings have been obtained on these structures using the PCM(DCM)-PBE0/cc-pVTZ approach. The tetramethylsilane reference signal was computed using the same protocol.

Issues with the original synthesis. The synthetic route originally to form **10** was to combine **7** with **5b** to form the intermediate **8** that, after further reaction with **7**, would provide **10** (Scheme 1 in the main text). However, following this strategy, the only compound obtained experimentally is **8.** We therefore used theory to rationalize this outcome assessing if the lack of reactivity of **8** could be explained by geometrical/steric and/or electronic effects. Note that in our calculations, the octyl chains were replaced by methyl groups for the sake of saving computational time.

We first performed conformational analyses for compound **8** and compared it to one of its ``reactive'' counterpart, **13**, the two *meta* NHR functions of **8** being replaced with a para-CO_2Me group in **13**. See below for an effective synthetic route extracted from a previous work.[14]

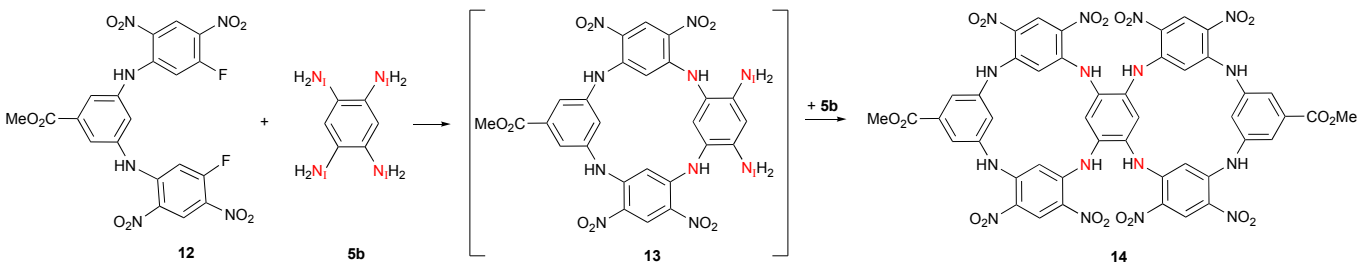

The optimized structures and relative stabilities are given in Figures **S13** and **S14** for **8** and **13**, respectively. It turns out that for both molecules, the most stable conformer is the usual 1,3-alternate structure, which is unsurprising. These conformations are denoted $\mathbf{X_i}$ in these Figures. Surprisingly, the amino functions of the ``reactive'' compound $\mathbf{13_i}$ actually seems less accessible than those of $\mathbf{8_i}$. Indeed, in the former, the distance between the carbon bearing the CO_2Me group and the opposite carbon located in between the two amino functions is 3.67 Å whereas a larger distance (of 4.26 Å) between the two atoms is computed in the latter non-reactive species. For the records, the same conclusions was obtained when re-optimizing both species without any dispersion corrections. Steric effects are therefore unlikely to

affect the reactivity of **8**, and one can reasonably conclude that the observed lack of reactivity is driven by electronic effects.

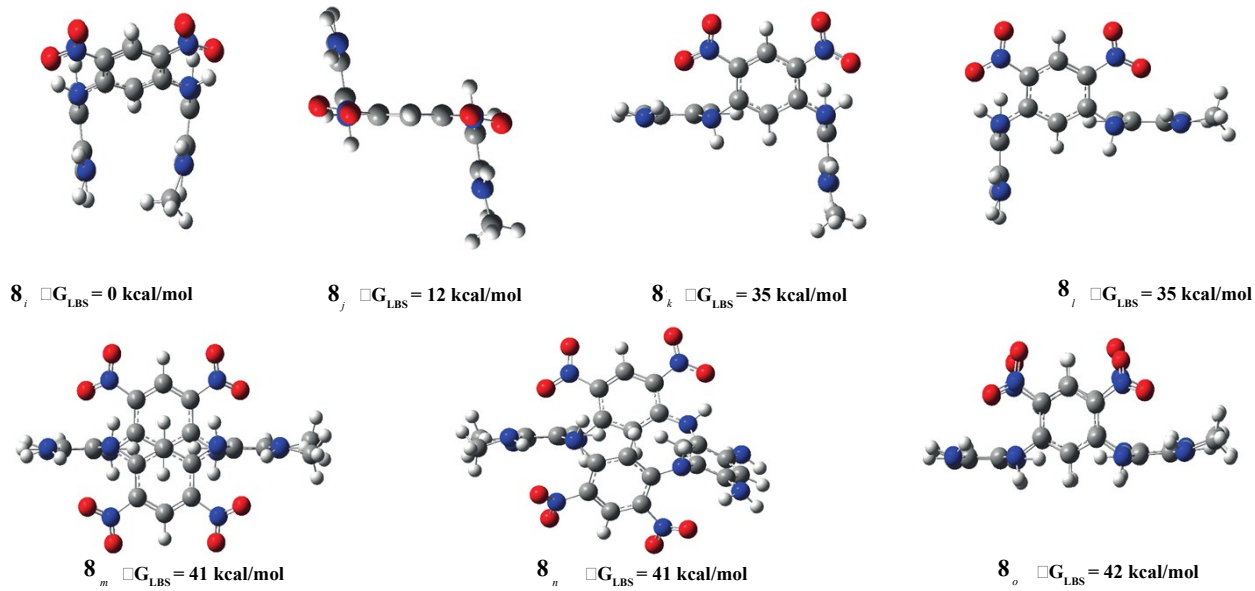

Fig. S13: Optimized conformers of **8** and their relative free energies corrected for basis set effects (ΔG^{LBS})

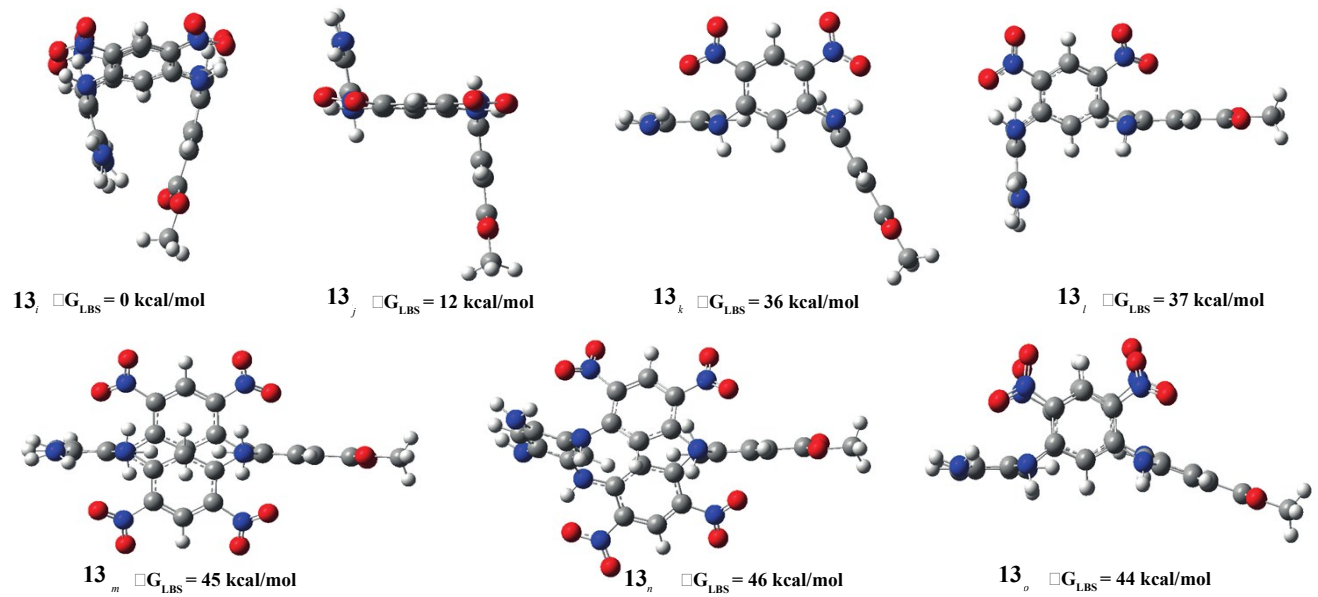

Fig. S14: Optimized conformers of **13** and their relative free energies corrected for basis set effects (ΔG^{LBS})

Consequently, we quantified electronic differences to explain the experimental observations. More specifically, we compared the nucleophilicity of the amino groups in **8** and in the selected ``reactive''

azacalix[4]arenes molecule, i.e., **13** for which it is indeed possible to reach the formation of its fused counterpart, **14**. The nucleophilicity of the amino groups in **5b** has also been evaluated. Theoretically, the estimation of the nucleophilicity of a specific site was achieved by using the well-known conceptual DFT approach, that consists in identifying the atoms undergoing the largest increase of charge when removing one electron from the neutral molecule. The partial atomic charges on the different compounds in both their neutral (Q=0) and cationic (Q=1) forms have therefore been computed. In Table **S1**, we report the MK charges of the nitrogen atoms of the primary and secondary external amino groups (denoted N_I and N_{II}, respectively, see scheme below) and their variations when removing one electron to the system. Note that the impact of the model used to compute the atomic charges was evaluated by using the CHelpG approach, but the obtained results (not shown) are similar to their MK counterparts, so that we discuss only the MK results here.

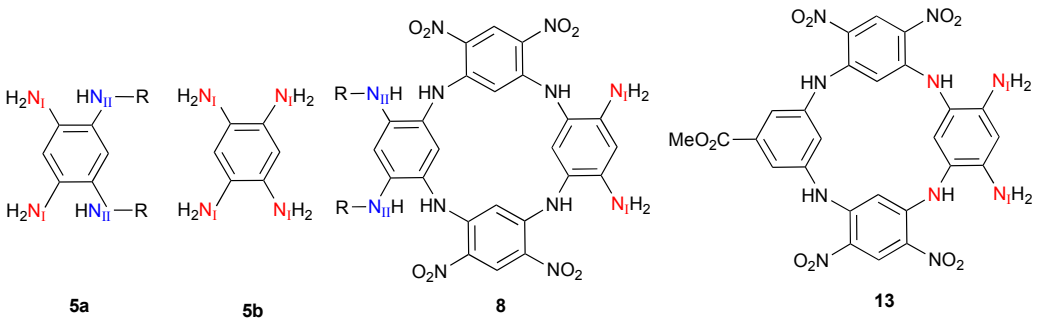

As seen in Table **S1**, for all species but **8**, i.e., for **5a**, **5b**, and **13**, one observes an increase of the charge on the nitrogen atoms (from +0.09 to +0.29 |e| depending on the molecule) when removing one electron to the system, on both the primary (N_I) and secondary (N_{II}) amines. A similar variation is obtained for the nitrogen atoms of the secondary amino groups (NHR) of **8** (+0.14 |e|) whereas the charge of the nitrogen atoms of the primary amino groups — that were expected to be ``reactive'' in the original reaction plan — surprisingly decreases (-0.09 |e|) when increasing the total charge of the molecule from 0 to +1. This clearly indicates that there is no nucleophilic character for the primary amino groups (NH_2) of **8**. This theoretical analysis is therefore explaining the experimental findings: **7** does not react with **8** to give the desired dimer, because the expected nucleophilic character of **8** is absent. Note that we have also performed additional calculations on the tetraaminophenyl **5a**, that reacts with **9** to form the dimer **10** and, consistently with the experiment, the four nitrogen atoms of **5a** present a nucleophilic character.

Table S1: Merz-Kollman charges (in |e|) of atoms N_I and N_{II} in selected structures in their neutral and cationic forms.

Molecule	Q_0 (N_I)	Q_1 (N_I)	ΔQ (N_I)	Q_0 (N_{II})	Q_1 (N_{II})	ΔQ (N_{II})
5a	-0.84/-0.85	-0.68/-0.69	+0.16	-0.47/-0.49	-0.34/-0.35	+0.14
5b	-0.79	-0.62	+0.17			
8	-0.63/-0.61	-0.72/-0.71	-0.09	-0.30	-0.15/-0.16	+0.14
13	-0.83/-0.76	-0.54/-0.67	+0.29/+0.09			

Conformation and NMR spectra of 10. Let us now present a conformational analysis for **10**. Indeed, for such molecule, it is difficult to know if only the conformation found in X-Ray should exist in another medium. The conformers of **10** have been generated from:

(i) combinations of the two most stable conformations of the monomer **8**, that is, $\mathbf{8_i}$ (ΔG=0 kcal/mol) and $\mathbf{8_j}$ (ΔG=12 kcal/mol) shown in Figure **S13**; and

(ii) the two optimized ACP dimers described afterwards.

The geometry optimizations of the ground state structures have been performed with and without accounting for dispersion corrections and the final structures are reported in Figures **S15** and **S16**, respectively, together with their relative free energies. Regarding first the results of Figure **S15** in which dispersion corrections have been accounted, it turns out that:

(i) the most stable structures possess two azacalix[4]arene moieties arranged similarly to the $\mathbf{8_i}$ conformation of Figure **S13**;

(ii) the most stable conformers have a S-like shape, the one the closest to the X-Ray one ($\mathbf{10_{ii}}$) being only less stable by 1.9 kcal/mol compared to the best structure found by DFT ($\mathbf{10_{ii'}}$), suggesting come flexibility in solutions;

(iii) all structures in which at least one azacalixarene moiety adopts a $\mathbf{8_j}$-like or other conformation are very unstable with relative free energies ranging from 8 to 30 kcal/mol.

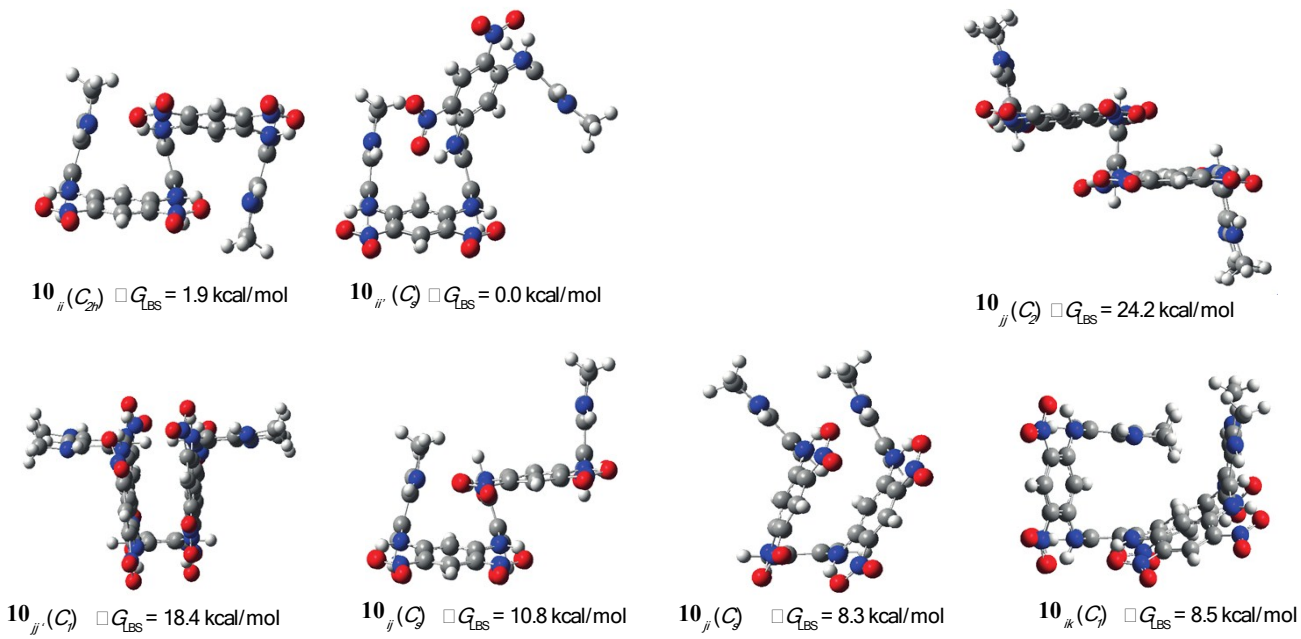

Fig. S15: Optimized conformers of **10** accounting for dispersion corrections with $D3^{BJ}$ and their relative free energies corrected for basis set effects (ΔG^{LBS})

Similar conclusions are obtained when dispersion corrections are not included (Figure **S16**) in the calculations although one notices that:

(i) the most stable form is $\mathbf{10_{ii''}}$, a conformer that could not be obtained when optimizing with dispersion correction, but remains obviously of the same S-shape as the structure found experimentally; and

(ii) the structures of Figure **S16** are, as expected, less ``compact'' compared to their dispersion-corrected counterparts of Figure **S15**.

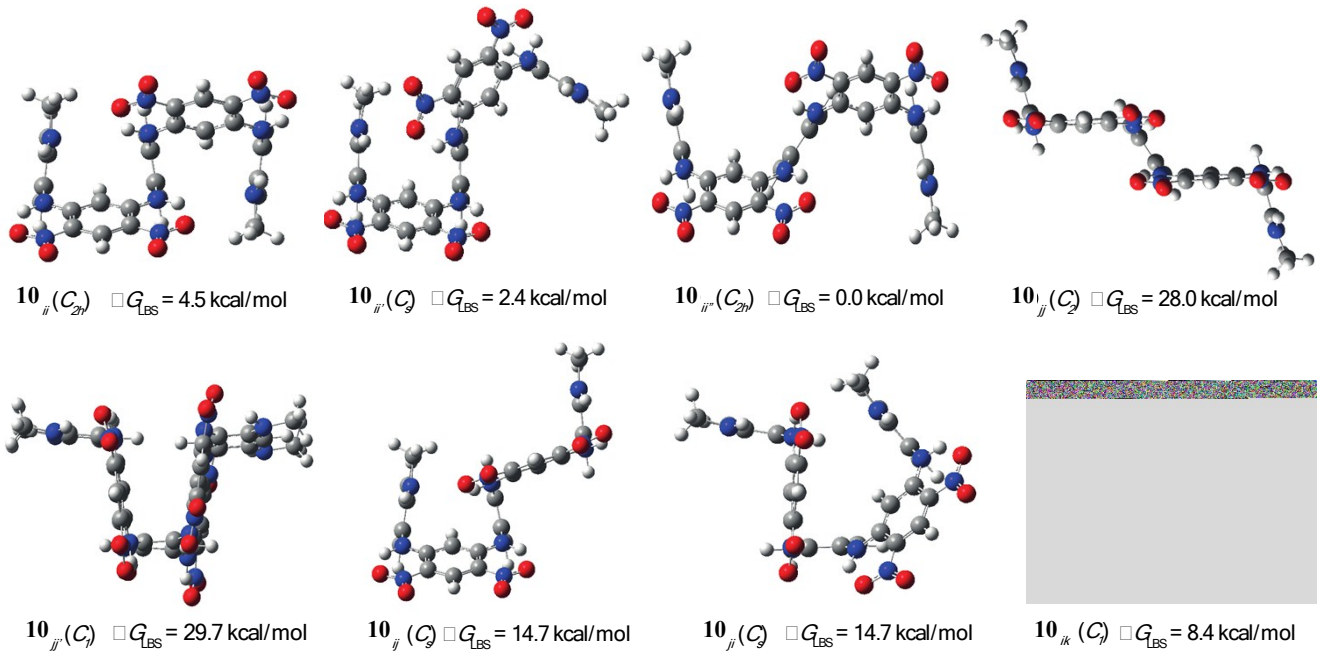

Fig. S16: Optimized conformers of **10** without accounting for dispersion corrections with D3^{BJ} and their relative free energies corrected for basis set effects (ΔG^{LBS})

The NMR spectra of the most stable dimer structures were also computed as they could be interesting to interpret the NMR spectrum of **10** (Figure **S4**) and evaluating the presence of one or more species in solution. The theoretical shieldings (computed at the PCM-PBE0/cc-pVTZ level of theory, replacing all long alkyl chains by methyl groups) are reported in Table **S2** and compared with the NMR signals of the protons of $\mathbf{8_i}$ obtained using the same computational protocol. Before analyzing these results, it is first worth noting that a NMR study of an azacalix[4]arene monomer analogue to **8**, i.e., in which the four external amino groups are all NHR groups with R=Me, denoted $\mathbf{8_{i\text{-}a}}$, has been performed following the very same protocol previously.[15] These results are reported in Table **S2** and a very good agreement between theoretical chemical shifts and the NMR measurements have been obtained (discrepancies smaller than 0.2 ppm) but for the external protons of the dinitrophenyl rings, namely H_a, and the protons of the bridging nitrogen atoms, namely H_f,with a DFT overestimation of the NMR shieldings of 0.6 and 0.9 ppm, respectively, compared to experiment. These larger yet acceptable discrepancies can easily be explained as these atoms are involved in hydrogen bonds with the oxygen atoms of the NO_2 groups. Indeed, these bonds are frozen in their optimized geometry, but at room temperature, the NO_2 groups are vibrating around their optimal positions.[15] Nevertheless, although the NMR chemical shifts of these protons are predicted to be overestimated compared to the measured ones, the evolutions of the shieldings from **8** to **10** should be reasonably well reproduced by theory, and we therefore focus on these changes below.

One first note that, as expected, similar NMR shieldings are computed for $\mathbf{8_i}$ (R=Me, R'=H) and $\mathbf{8_{i\text{-}a}}$ (R=R'=Me), the most important effect being obtained for the external protons of the diaminophenyl ring (+0.4 ppm). When turning to **10**, one sees that the deformation of the structure from $\mathbf{10_{ii}}$ to $\mathbf{10_{ii''}}$ leads to interesting variations. Indeed, comparing with the monomer, identical chemical shifts are obtained for H_d protons whereas different trends can be observed for the H_a, H_b, H_c, H_e, and H_f. For these latter protons,

theory provides smaller (larger) chemical shifts in the **10$_{ii}$** (**10$_{ii}$"**) conformations, and the reverse trend is observed for H_c protons. However, one can reasonably think that the **10$_{ii}$**-like structures are rapidly interchanging in solution and that the measured NMR signal should correspond to the mean proton signals between these structures. Indeed, calculations indicate that the ``opening/closing'' of the diaminophenyl branches, i.e, going from **10$_{ii}$** to **10$_{ii}$'**, requires less than 2 kcal/mol, hinting that both structures exchange in solution. Regarding the trends from **8** to **10**, theory predicts rather similar proton shieldings for H_a, H_b, H_c, H_d, and H_f (with a maximal shift of 0.3 ppm), as well as the apparition of two new signals on the NMR spectrum:

(i) a signal integrating for the two central hydrogen atoms, H_e, that is predicted to peak at 7.7 ppm; and

(ii) a signal integrating for the four protons of the bridge H_g, that is predicted to be separated from the H_f signal by 0.2 ppm.

We report in Table **S2** a comparison between the theoretical signals and the measured ones. Regarding first the mean shieldings accounting for the three **10$_{ii}$** -like structures, as observed for the monomer, it turns out that:

(i) theory predict systematically larger chemical shielding than experiment;

(ii) the internal protons (H_b, H_d, and H_e) and the external protons of the diaminophenyl rings (H_c) are providing errors smaller than 0.5 ppm; and

(iii) larger errors, 0.6 and 0.8 ppm, are obtained for external protons of the dinitrophenyl rings (H_a) and protons of the bridge (H_f and H_g).

Finally, let us compare the measured and experimental NMR signals of each **10** conformer. For **10$_{ii}$"** , a too large error (+0.9 ppm) for the H_b protons that should be well described by theory. For **10$_{ii}$**, although the MAE is small (0.3 ppm), theory predicts the reverse trend for the H_b protons when going from the monomer to the dimer, i.e. -0.2 ppm instead of +0.2 ppm experimentally. For **10$_{ii}$'**, a very good match with experiment is obtained, thus indicating that this conformer should be dominant in solution, though again an exchange between the three **10$_{ii}$** -like structures is likely to occur.

Table S2: Theoretical (th.) NMR proton shieldings (in ppm) of the most stable **8** and **10** optimized at the PCM(DCM)-PBE0-D3^{BJ}/6-31G(d) level of theory except when explicitly noted. When available, the experimental (exp.) data are also given as well as the theoretical error (Δ) and mean absolute error (MAE).

Molecule		H_a	H_b	H_c	H_d	H_e	H_f	H_g	MAE
8$_{i-a}$	Exp.	9.3	5.5	5.8			8.9		
	Th.	9.9	5.5	5.9			9.8		
	Δ	0.0	0.0	0.1			0.9		0.4
8$_{i}$	Th.	9.9	5.5	6.2	6.9		9.7		
10	Exp	9.3	5.7	5.9	6.7	7.4	9.0	9.2	
10$_{ii}$	Th.	9.7	5.3	6.3	7.1	7.5	9.4	9.4	
	Δ	0.4	-0.4	0.4	0.4	0.1	0.4	0.2	0.3
10$_{ii}$'	Th.	10.0	5.7	5.9	6.9	7.7	9.9	10.1	
	Δ	0.7	0.0	0.0	0.2	0.3	0.9	0.9	0.4
10$_{ii}$"[a]	Th.	10.0	6.6	6.1	7.1	7.8	10.1	10.6	
	Δ	0.7	0.9	0.2	0.4	0.4	1.1	1.4	0.7
10$_{ii}$"-like[b]	Th.	9.9	5.8	6.1	7.0	7.7	0.8	10.0	
	Δ	0.6	0.1	0.2	0.3	0.3	0.8	0.8	0.4

[a] The NMR calculation has been performed on the structure optimized at the PCM(DCM)-PBE0/6-31G(d) level of theory, without any dispersion corrections.

[b] The reported data correspond to the mean values obtained for the three conformers reported here.

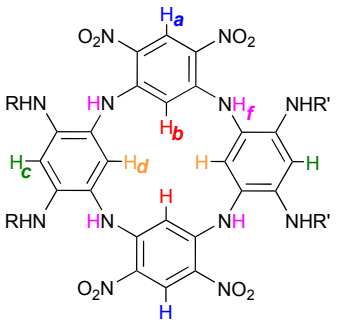

8$_i$: R=Alkyl, R'=H
8$'_i$**-a**: R=R'=Alkyl

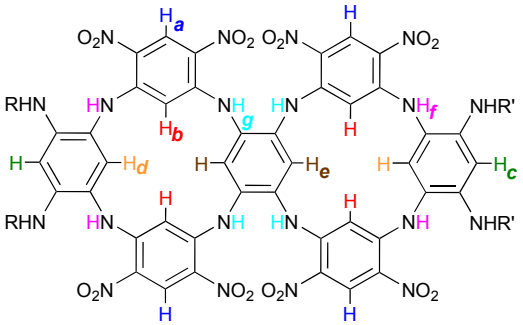

10 R=R'=Alkyl

Theoretical Section: structure and properties of **4**

We have performed calculations on a simplified form of **4**, in which the side octyl rings have been neglected for the sake of saving computational time. In the following, to clearly distinguish this structure, we will simply name it **AD** (azacalixphyrin dimer). We have considered the different protonation states displayed in Figure **S17** and we describe the structure, aromaticity, and optical properties of these compounds and compare the data with those obtained for the monomer species.

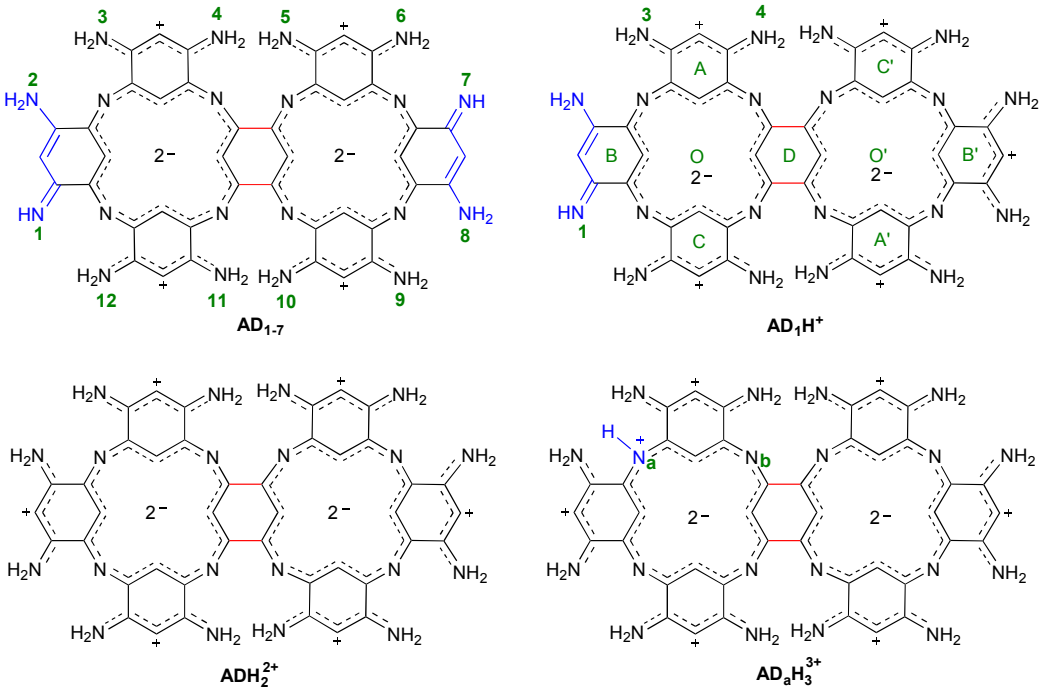

Fig. S17: Representation of the equivalent of **4** in several protonation states. The changes upon protonation/deprotonation of the di-protonated $\mathbf{ADH_2^{2+}}$, that we use as reference, are highlighted in blue. The displayed neutral form (top left) has two imine groups at position 1 and 7 and is hence noted $\mathbf{AD_{1\text{-}7}}$. The NICS centers (and phenyl rings labels) are indexed using capital letters (O, A, B, C, and D) on the **AD** structure, the different imine/amine functions (bridging nitrogen atoms) are labeled from 1 to 12 (a and b) on the $\mathbf{ADH^+}$ ($\mathbf{ADH_3^{3+}}$) structure. The CC distances that link the two ACP centers are highlighted in red.

Methods. All DFT and TD-DFT calculations have been achieved using the Gaussian09/16 programs.[9] The optimization and frequency calculations have been performed at the PBE0[10]/6-31G(d) level of theory. The self-consistent field (10^{-10} a.u.) and geometry optimization (10^{-5} a.u.) convergence thresholds have been tightened and the (99,590) pruned integration grid (the so-called *ultrafine* grid) has been used. DFT Hessian were computed to confirm the nature (minima) of all ground state (GS) structures and to access to the free energy (*G*) of each structures. On the basis of the optimized structures, we computed:

(i) single point calculations using the D3 version of Grimme's dispersion approach with Becke-Johnson damping ($D3^{BJ}$)[11] for **4** using the same level of theory as for the optimization and frequency calculations;

(ii) the NICS(0) computed in gas phase at the PBE0/cc-pVTZ level of theory; [16]

(iii) the total and transition energies (40 states) using the PBE0[10] and CAM-B3LYP[17] exchange-correlation functionals in combination with the larger 6-311+G(2d,p) atomic basis set (LBS).

Except when explicitly noted, the solvent (DMSO) has been accounted in all the calculations by using the polarizable continuum model (PCM)[18] approach in its linear-response (LR) form, under its *non-equilibrium* limit for excitation calculations.

Conformers and tautomers. In view of the saddle shape of the ACP monomers,[19] two conformations have been envisioned. Indeed, for all the protonated and non-protonated dimer structures, the S-shaped and U-shaped conformers, displayed in Figure **S18**, have been modeled. While the symmetric C_{2h} S-shaped structure was found to be a true minimum, the U-shaped structure in the expected C_{2v} point group returned two imaginary frequencies, the minimum structure adopting a C_s point group.

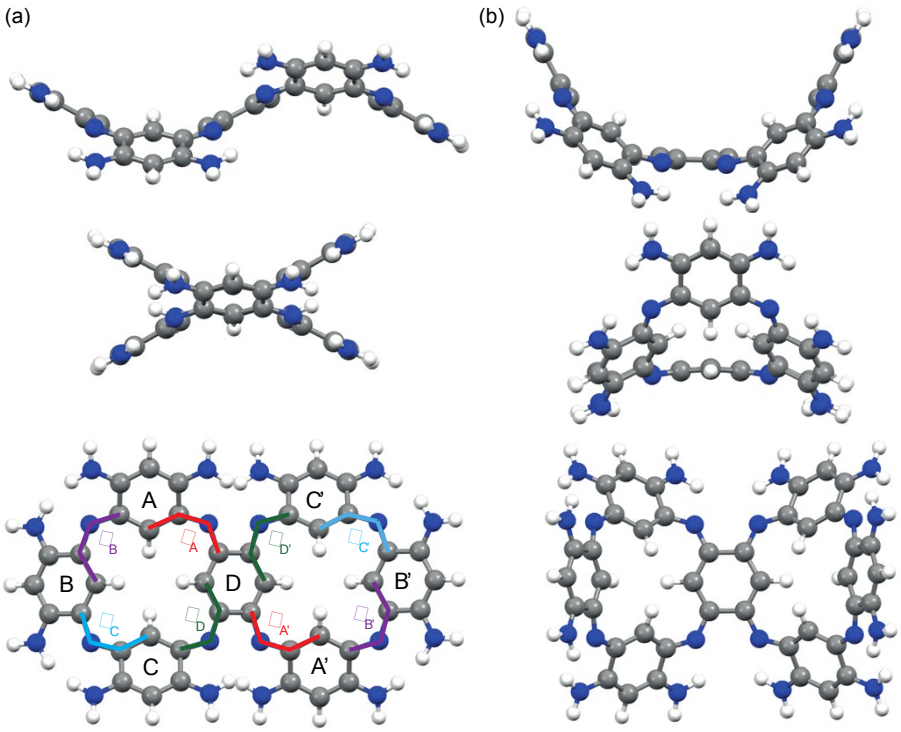

Fig. S18: Side (top and middle) and top (bottom) views of the optimized (a) S-shaped and (b) U-shaped conformers of $\mathbf{ADH_2^{2+}}$. The former (latter) exhibits a C_{2h} (C_s) symmetry point group. The label of the phenyl-like rings (A, B, C, D, A', B', and C') and key dihedral angles (ϕ_X, X being the label of the phenyl-like ring) are displayed on the ACP structure in the top view of the S form.

First, it is worth commenting on the ``Lewis'' structures represented in Figure **S17**, and more particularly, on the nature of the CC bond shared by the two macrocycles (highlighted in red in that Figure). Indeed, in all the optimized structures, irrespective of their conformation or protonation state, these CC bonds are 1.47-1.49 Å long, which clearly indicates that both centers are linked through CC bonds presenting a dominant single character and are therefore mostly uncoupled in the electronic ground state. This is reminiscent of what can be found for ACP.[19]

The relative stabilities of the different tautomers and conformers of the protonated and non-protonated azacalixphyrin dimers calculated at the PCM(DMSO)-PBE0/6-31G(d) level are displayed in Figure **S19**. For a given tautomer, the S-shaped conformation systematically yields more stable structures than the U-shaped conformation but for the $\mathbf{AD_{1\text{-}3}}$ tautomer. Concerning the most-protonated species, $\mathbf{ADH_3^{3+}}$, it turns out that $\mathbf{AD_aH_3^{3+}}$ is much less stable than $\mathbf{AD_bH_3^{3+}}$ in both S and U forms, the difference exceeding 10 kcal/mol. Indeed, in $\mathbf{AD_bH_3^{3+}}$, the additional proton is stabilized by the lone pair of the nearby

bridging nitrogen atom. For the di-protonated $\mathbf{ADH_2^{2+}}$, both S- and U-shaped structures might co-exist in solution as their free energy differ by less than 2 kcal/mol. For the mono-protonated compounds, $\mathbf{ADH^+}$, all structures present free energies that does not differ by more than 3.2 kcal/mol and it is therefore highly likely that several tautomers co-exist in solution. Concerning the non-protonated species, consistently with the study performed for the ACP,[19] tautomers presenting two imine functions on the same phenyl ring, i.e., $\mathbf{AD_{1\text{-}2}}$ and $\mathbf{AD_{3\text{-}4}}$, are not stable; they present free energies that are ca. 20 kcal/mol above the most stable structure. Among all the tautomers, eighteen present a relative free energy within 3 kcal/mol of the most stable form. As this number is huge, we decided to study the aromaticity and the optical properties in the following considering ``only'' the nine most stable tautomers, that is the S-shaped $\mathbf{AD_{1\text{-}6}}$, $\mathbf{AD_{1\text{-}9}}$, $\mathbf{AD_{3\text{-}5}}$, $\mathbf{AD_{3\text{-}6}}$, $\mathbf{AD_{3\text{-}9}}$, $\mathbf{AD_{3\text{-}10}}$, $\mathbf{AD_{4\text{-}5}}$, and $\mathbf{AD_{4\text{-}10}}$, as well as the U-Sahped $\mathbf{AD_{3\text{-}10}}$, that all possess relative free energies within a 1.3 kcal/mol window (*vide infra*).

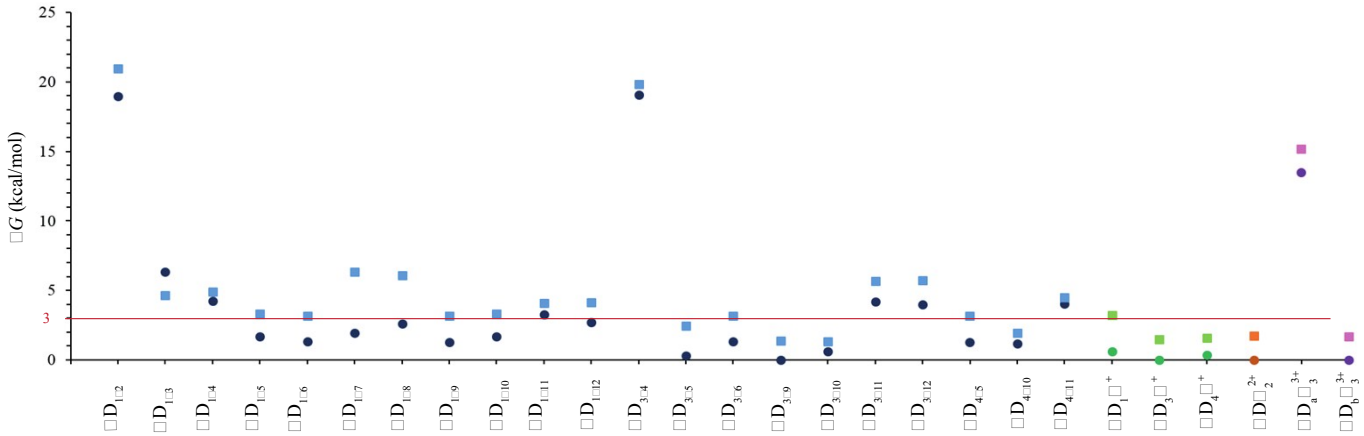

Fig. S18: Relative stabilities (ΔG in kcal/mol) computed at the PCM(DMSO)-PBE0/6-31G(d) level of theory for the S-shaped (circles) and U-shaped (squares) conformers and the possible tautomers of the different structures of the ACP dimer: **AD** (blue), $\mathbf{ADH^+}$ (green), $\mathbf{ADH_2^{2+}}$ (orange), and $\mathbf{ADH_3^{3+}}$ (violet). The most stable form is used as reference. The horizontal red line indicates the 3 kcal/mol threshold.

Although the U-shaped structures present an energy close to the one of their S-shaped counterparts, this does not necessarily mean that the two conformers are actually present in the experimental pot. Indeed, the energetic barrier for going from one conformation to another is likely to be high, thus indicating that once a conformer is formed in solution, it keeps its structural conformation at room temperature. The synthetic route leading to the compound is consequently crucial. Indeed, it is also possible that several conformers of the precursor species co-exist in solution and yield an unconvertible mixture of S and U forms after the reaction. In the previous, the conformational analysis on **10** suggested that only ``S-like'' structures were thermodynamically stable. Therefore, at this stage, we reasonably predict that the U-shaped **AD** (and hence **4**) are not experimentally formed, but it remains too risky to exclude definitively their presences as it is possible that chemical substitution impacts the structural arrangement or that complex changes take place during the reaction. This is why we present the results for both conformations in the following.

Aromaticity. We then characterized the global aromaticity of the constituting six-membered rings as well as of the two macrocyclic centers of **AD**. The NICS(0) values at the centers (O and O', see labels on Figure **S16**) are reported in Table **S3** together with the dihedral angles ϕ (see Figure **S17**) that reflects the deviation of the macrocycle from planarity.

It turns out that both centers of the **AD** derivatives present a strong aromatic character (negative NICS values), the absolute NICS values being ordered as follows: **AD** ~ $\mathbf{ADH^+}$ < $\mathbf{ADH_2^{2+}}$. For the tri-protonated molecule, while the center O' also present a strong aromatic character, the global aromaticity of the macrocycle comprising the protonated bridge, center O, is found to be much less aromatic. This can be explained by the fact that in $\mathbf{AD_bH_3^{3+}}$, the differences between the ϕ_A and ϕ_C in the S or U conformations respectively reaches 10 or 12°, that is, protonation strongly deforms the structure. One observes that the absolute NICS values are systematically larger in the S-shaped forms than in their U-shaped counterpart, i.e., the global aromaticity (centers O and O') of the S-shaped compounds is larger than in their U-shaped analogues. This is consistent with, on the one hand, the relative stabilities reported in Figure **S18**, and, on the other hand, the ϕ angles that largely deviates from one another inside a given macrocyclic unit adopting the U conformation, whereas smaller deviations are found in the S-shaped one. Note here that the NICS values of the constitutive phenyl-like rings (not listed here), indicate that these rings present an anti- or non-aromatic character as expected from the results of the "monomer" ACP (**1**).[19] The ring D is the most anti-aromatic [NICS(0)] with values between 6.8 and 10.1 ppm, which is perfectly consistent with its position in the dimer: this phenyl-like ring is shared by the two macrocycles.

Table S3: Global aromaticity and selected and geometrical parameter in several dimer structures. The reported NICS(0) values (in ppm) are given for centers O and O', that corresponds to the center of each ACP moiety in a dimer structure. The reported distances (in Å) and angles (in degrees) are represented in Figure **S13**. To allow a direct comparison with the "monomer" molecule, the data for the di-protonated ($\mathbf{1.H_2^{2+}}$).Hare given as well.

		NICS(O)	NICS(O')	ϕ_A	ϕ_B	ϕ_c	ϕ_D	ϕ_A'	ϕ_B'	ϕ_c'	ϕ_D'
$\mathbf{1.H_2^{2+}}$		-8.4		22	22	22	22				
$\mathbf{ADH_2^{2+}}$	S	-7.0	-7.0	20	22	20	24	20	22	20	24
	U	-6.3	-6.3	22	23	21	23	22	23	22	26
$\mathbf{AD_bH_3^{3+}}$	S	-4.5	-7.6	26	22	18	25	22	22	20	22
	U	-2.8	-7.1	30	22	19	24	22	22	21	24
$\mathbf{AD_1H^+}$	S	-6.1	-5.4	22	19	21	25	20	23	20	26
	U	-5.7	-3.6	23	18	21	28	21	23	20	27
$\mathbf{AD_3H^+}$	S	-5.3	-6.0	18	23	23	22	20	23	19	24
	U	-4.7	-4.7	21	23	23	17	22	24	20	19
$\mathbf{AD_4H^+}$	S	-5.2	-6.4	22	27	22	22	20	23	20	24
	U	-4.8	-5.4	25	28	21	18	23	24	19	19
$\mathbf{AD_{1-6}}$	S	-6.5	-4.8	23	17	22	26	25	21	21	31
$\mathbf{AD_{1-9}}$	S	-6.6	-4.8	21	17	22	25	18	23	23	23
$\mathbf{AD_{3-5}}$	S	-5.2	-4.8	19	23	23	22	22	24	19	25
$\mathbf{AD_{3-6}}$	S	-6.2	-4.9	19	23	23	23	24	21	20	29
$\mathbf{AD_{3-9}}$	S	-5.1	-5.1	17	22	23	21	17	22	23	21
$\mathbf{AD_{3-10}}$	S	-5.3	-4.8	18	22	23	21	21	27	21	22
$\mathbf{AD_{3-10}}$	U	-4.6	-4.4	20	23	23	17	24	28	21	17
$\mathbf{AD_{4-5}}$	S	-4.9	-4.9	23	28	21	23	22	23	19	26
$\mathbf{AD_{4-10}}$	S	-5.0	-5.0	21	26	21	21	21	26	21	21

Optical properties. We now turn towards the optical properties of the dimer species. The theoretical absorption spectra of the energetically probable dimer structures in different protonation states are given in Figure **S20**. As mentioned above, due to the large number of possible neutral forms, the electronic transitions have not been computed for all species but for the nine most stable tautomers ``only''. One first observes a systematic bathochromic shift of both the first (NIR) and second (at ca. 600 nm) absorption bands compared to the monomer, i.e., strong red-shifts are predicted when extending the π-conjugation of these systems. This holds irrespective of the protonation state and this effect is even more pronounced for the least stable U-shaped conformers than for its S-shaped counterpart. As stated in the Introduction, merging ACPs aimed at red-shifting the absorption of the parent monomer by extending its π - conjugation path which is clearly confirmed by the delocalized π (π*) molecular orbitals of the di-protonated $\mathbf{ADH_2^{2+}}$ depicted in Figure **S21** and occurs despite the single bond character of the connecting CC bonds. In that Figure, the energies and topologies of the orbitals involved in the NIR band of the S-shaped $\mathbf{ADH_2^{2+}}$ are shown and compared with the parent ACP monomer ($\mathbf{1.H_2^{2+}}$=$\mathbf{AH_2^{2+}}$)

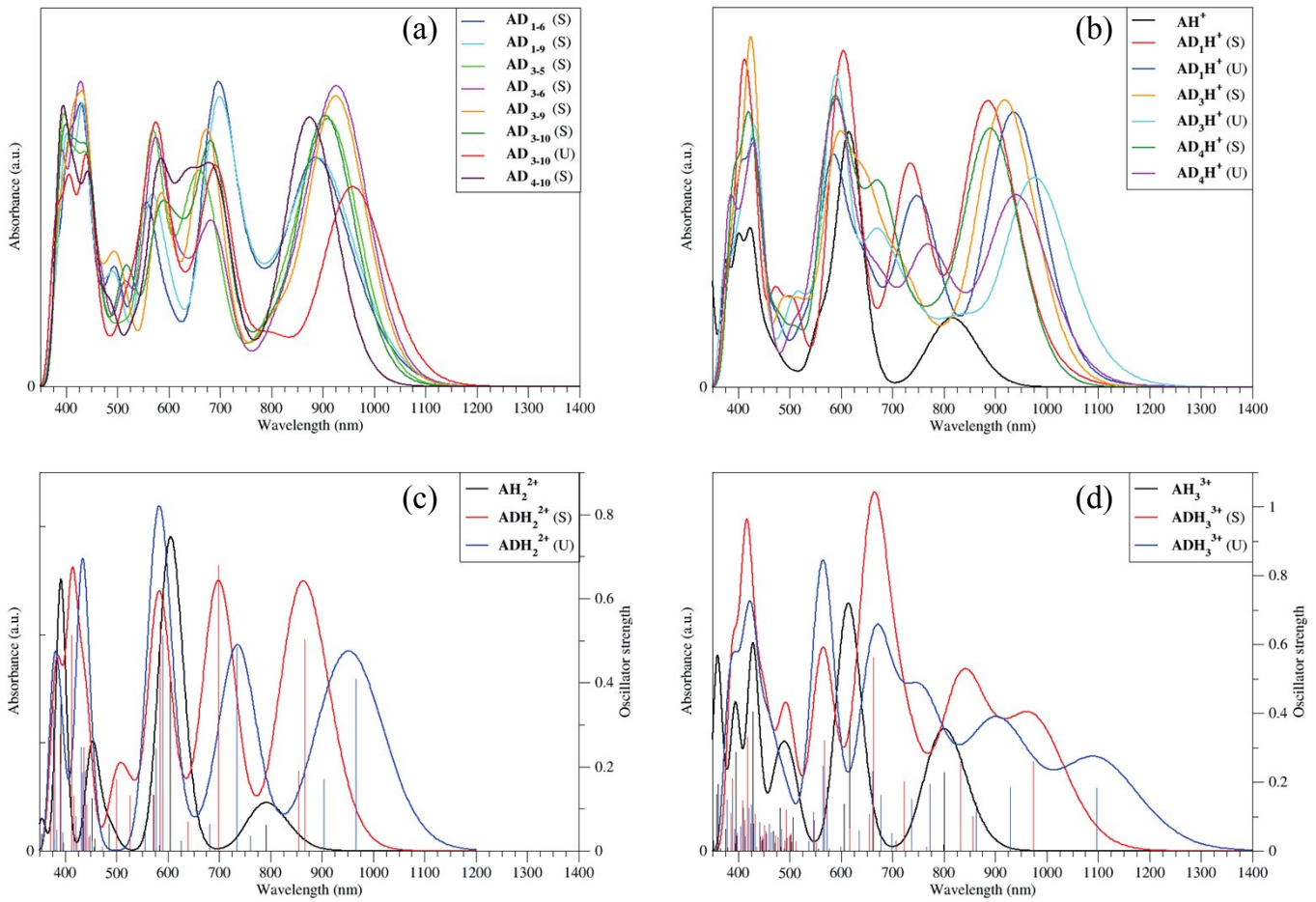

Fig. S20: Theoretical [PCM-PBE0/6-311+G(2d,p)] absorption spectra of (a) the nine most stable forms of the non-protonated **AD**; (b) $\mathbf{ADH^+}$; (c) $\mathbf{ADH_2^{2+}}$; and (d) $\mathbf{ADH_3^{3+}}$ with S and U shapes indicated in parenthesis. For the protonated species, the spectrum of the corresponding monomer counterpart is reported in black for comparisons. The sticks have been convoluted with a Gaussian function with a FWHM of 1500 cm^{-1}. For the sake of clarity, the sticks have been omitted in panels (a) and (b).

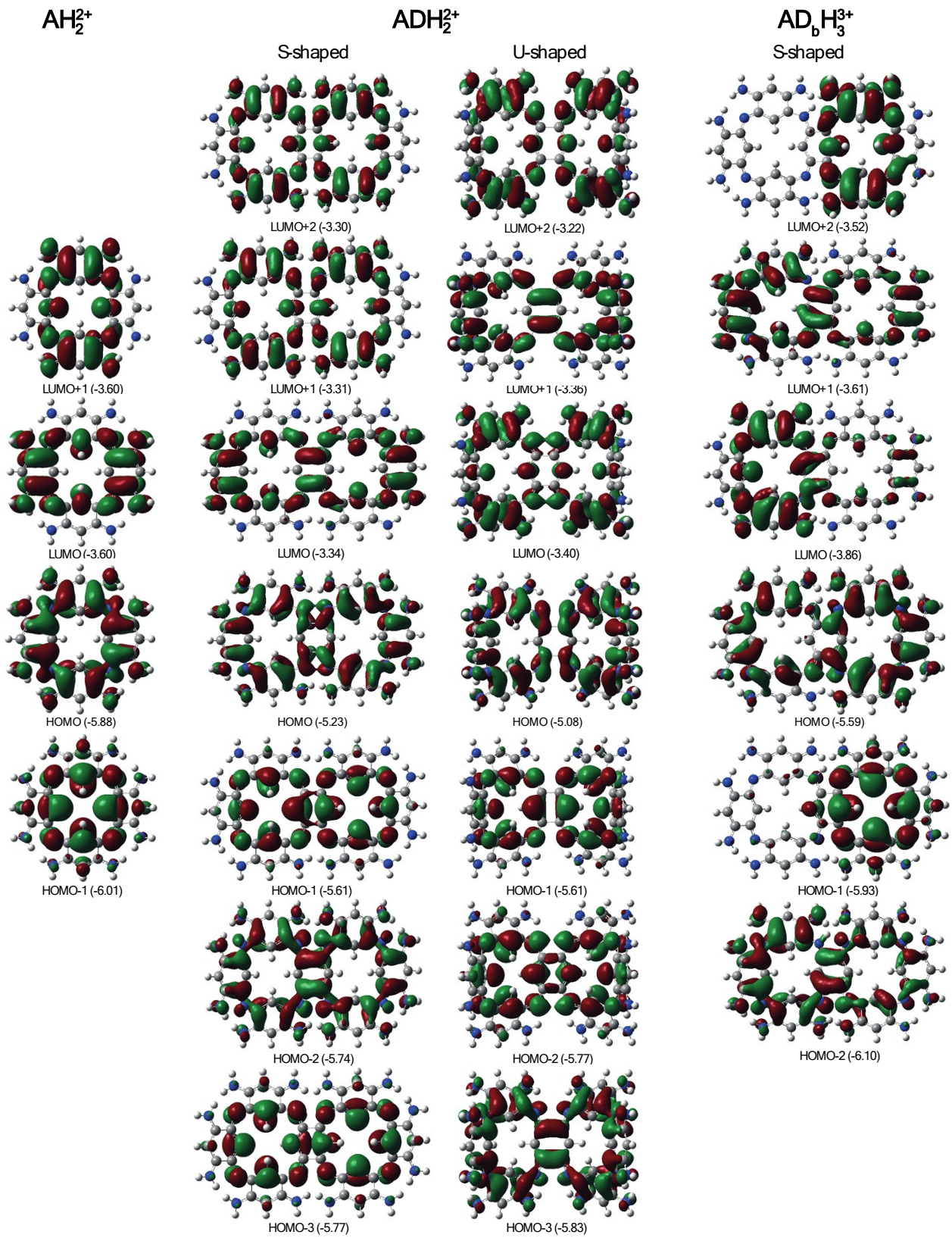

Fig. S21: Molecular orbitals (isovalue= 0.02 a.u.) involved in the first dipole-allowed electronic transitions of the S-/U-shaped $\mathbf{ADH_2}^{2+}$ and S-shaped $\mathbf{ADH_3}^{3+}$. A comparison with the MO of the $\mathbf{1.H_2}^{2+}$ ($\mathbf{AH_2}^{2+}$) monomer is provided on the left-hand side. The energies (in eV) of each orbital are given in parenthesis.

The transition energies, oscillator strengths, and contributions of the molecular orbitals in the first strongly-dipole allowed excitations are reported in Table **S4**. Looking at the energies of the frontier orbitals in Figure **S21**, one notices that they are all destabilized upon fusion of two macrocycles, this destabilization being pronounced for the HOMO (+0.65 eV) and HOMO-1 (+0.40 eV). As a consequence, the gap between the occupied and unoccupied orbitals decreases which is perfectly consistent with the redshifted spectra predicted by TD-DFT. Similar trends are obtained for the U-shaped conformer (see Figure **S20**), the destabilization of the HOMO being even more pronounced (+0.80 eV compared to the monomer) which again matches perfectly the fact that U-shaped conformers systematically absorbs at lower energies than their S-shape analogues. Moreover, comparing the spectra in Figure **S19c**, one observes, in contrast to the ACP monomer:

(i) very intense transitions in the 700-1000 nm region; and

(ii) a lifting of the degeneracy between the two excited state pairs.

The S_2/S_3 states involved in the NIR band remain rather close in energy (with a gap smaller than 0.1 eV) whereas a larger gap (of 0.3-0.4 eV) is obtained between the S_6 and S_{13} states that are mainly responsible for the bands in the visible domain. Therefore not only the calculations predict a redshift of the NIR band but also a broader and more intense absorption for the $\mathbf{ADH_2^{2+}}$ dimer than for $\mathbf{AH_2^{2+}}$. Asa final note, to ensure that the optical properties are qualitatively well-described using the PBE0 functional, we computed the spectra using CAM-B3LYP functional for both di- and tri-protonated species and obtained similar signatures with this latter functional (not listed here), the only noticeable qualitative difference being the blueshift of the bands compared to the PBE0 spectra, a change that is usual when going to functionals comprising more \ *exact*-like exchange.

Table S4: Theoretical absorption energies (λ_{abs} in nm), oscillator strengths (*f*), and contributions of the molecular orbitals involved in the first four strongly dipole-allowed transitions ($f > 0.1$) for the $\mathbf{ADH_2^{2+}}$ and S-shaped $\mathbf{ADH_3^{3+}}$ species using the PBE0 functional. H and L stand for HOMO and LUMO, respectively.

	Shape	State	λ_{abs}	*f*	Orbitals
$\mathbf{1.H_2^{2+}}$		1 & 2	791	0.12	H–1→L (26%), H–1→L+1 (26%), H→L+1 (24%), H→L (24%)
		3 & 4	506	0.80	H→L (25%), H→L+1 (25%), H–1→L (23%), H–1→L+1 (23%)
$\mathbf{ADH_2^{2+}}$	S	2	866	0.50	H→L (78%), H–1→L+1 (15%)
		3	855	0.19	H→L+2 (81%), H–3→L (14%)
		6	699	0.68	H–1→L+1 (75%), H→L (20%)
		13	585	0.55	H–3→L (58%), H–2→L+1 (31%)
$\mathbf{ADH_2^{2+}}$	U	2	966	0.41	H→L+1 (85%), H–1→L (12%)
		3	903	0.17	H→L+2 (85%), H–2→L+1 (12%)
		5	735	0.48	H–1→L (82%), H→L+1 (14%)
		11	589	0.51	H–2→L+1 (48%), H–3→L (40%)
$\mathbf{ADH33^{+}}$	S	1	973	0.26	H→L (92%)
		2	856	0.10	H–1→L (39 %), H→L+2 (35 %), H–1→L+1 (11 %)
		3	832	0.26	H→L+1 (69 %)
		5	723	0.20	H–2→L (41%), H–1→L (15%), H→L+2 (15%)

References

1. a) H. S. Nalwa, T. Watanabe, K. Ogino and S. Miyata, *J. Mater. Sci.*, 1998, **33**, 3699; b) C. Seillan and O. Siri, *Tetrahedron Lett.*, 2009, **50**, 630.

2. Z. Chen, R. Haddoub, J. Mahé, G. Marchand, D. Jacquemin, J. Andeme Edzang, G. Canard, D. Ferry, O. Grauby, A. Ranguis and O. Siri, *Chem. Eur. J.*, 2016, **22**, 17820.

3. COLLECT, Nonius BV, Delft, The Netherlands, **2001**.

4. Z. Otwinowski and W. Minor, in *Methods in Enzymology. In Macromolecular Crystallography, Part A*, ed. C. W. Jr. Carter and R. M. Sweet, Academic Press: New York, 1997, vol. 276, p. 307.

5. A. Altomare, G. Cascarano, G. Giacovazzo, A. Guagliardi, M. C. Burla, G. Polidori and M. Camalli, *J. Appl. Crystallogr.*, 1994, **27**, 435.

6. G. M. Sheldrick, *Acta Crystallogr. A*, 2015, **C71**, 3.

7. O. V. Dolomanov, L. J. Bourhis, R. J. Gildea, J. A. K. Howard and H. Puschmann, *J. Appl. Crystallogr.*, 2009, **42**, 339.

8. G. M. Sheldrick, *Acta Crystallogr. A*, 2015, **A71**, 3.

9. M. J. Frisch, et al., Gaussian 09 Revision D.01./Gaussian 16 Revision A.03 Gaussian Inc. Wallingford CT, 2009 & 2016.

10. C. Adamo and V. Barone *J. Chem. Phys*. 1999, **110**, 6158

11. S. Grimme, S. Ehrlich and L. Goerigk *J. Comput. Chem*. 2011, **32**, 1456.

12. U. C. Singh and P. A. Kollman, *J. Comput. Chem*. 1984, **5**, 129.

13. C. M. Breneman and K. B. Wiberg, J. *Comput. Chem*. 1990, **11**, 361.

14. G R. Haddoub, M. Touil, Z. Chen, J.-M. Raimundo, P. Marsal, M. Elhabiri and O. Siri, *Eur. J. Org. Chem.*, 2014, 745.

15. Z. Chen, G. Canard, C. Azarias, D. Jacquemin and O. Siri, *New J. Chem*. 2017, **41**, 5284.

16. Z. Chen, C. S. Wannere, C. Corminboeuf, R. Puchta and P.v.R. Schleyer, *Chem. Rev.* 2005, **105**, 3842.

17. J. Tomasi, B. Mennucci, and R. Cammi, *Chem. Rev*. 2005, **105**, 2999.

18. T. Yanai, D. P. Tew and N. C. Handy, *Chem. Phys. Lett*. 2004, **393**, 51.

19. Z. Chen, M. Giorgi, D. Jacquemin, M. Elhabiri and O. Siri, *Angew. Chem. Int. Ed.*, 2013, **52**, 6250.